



LUND UNIVERSITY  
Faculty of Medicine

---

# LUP

*Lund University Publications*  
Institutional Repository of Lund University

---

This is an author produced version of a paper published in Cell. This paper has been peer-reviewed but does not include the final publisher proof-corrections or journal pagination.

Citation for the published paper:

Gokul Kesavan, Fredrik Wolfhagen Sand, Thomas Greiner, Jenny Johansson, Sune Kobberup, Xunwei Wu, Cord Brakebusch, Henrik Semb

"Cdc42-mediated tubulogenesis controls cell specification."

Cell, 2009 139 (4) 791 - 801

<http://dx.doi.org/10.1016/j.cell.2009.08.049>

Access to the published version may require journal subscription.

Published with permission from: Elsevier Cell Press

# Cdc42-mediated tubulogenesis controls cell specification

Gokul Kesavan<sup>1</sup>, Fredrik Wolfhagen Sand<sup>1</sup>, Thomas Uwe Greiner<sup>1</sup>, Jenny Kristina Johansson<sup>1</sup>, Sune Kobberup<sup>1</sup>, Xunwei Wu<sup>2</sup>, Cord Brakebusch<sup>2</sup>, Henrik Semb<sup>1\*</sup>

<sup>1</sup>Stem Cell and Pancreas Developmental Biology, Stem cell center, Lund University, BMC, SE-22184 Lund, Sweden

<sup>2</sup>Biomedical Institute, BRIC, University of Copenhagen, 2100 Copenhagen, Denmark

\*Correspondence: [Henrik.Semb@med.lu.se](mailto:Henrik.Semb@med.lu.se)

## SUMMARY

Understanding how cells polarize and coordinate tubulogenesis during organ formation is a central question in biology. Tubulogenesis often coincides with cell lineage specification during organ development. Hence, an elementary question is whether these two processes are independently controlled, or whether proper cell specification depends on formation of tubes. To address these fundamental questions, we have studied the functional role of Cdc42 in pancreatic tubulogenesis. We present evidence that Cdc42 is essential for tube formation, specifically for initiating microlumen formation and later for maintaining apical cell polarity. Finally, we show that Cdc42 controls cell specification non-cell-autonomously by providing the correct microenvironment for proper control of cell fate choices of multipotent progenitors.

## INTRODUCTION

Organs such as the lung, kidney, pancreas, salivary gland and mammary gland are primarily made up of tubes that act as biological pipes for transporting vital fluids

and gases. Two principle mechanisms for mammalian tubulogenesis have been described. One mechanism involves reiterative sprouting and stereotypical branching of a tubular anlagen consisting of fully polarized epithelial cells. This process has for example been described in the lung (Metzger et al., 2008). The other mechanism is represented in glandular organs, e.g. the pancreas, mammary gland, prostate and salivary glands, where tubulogenesis arises when groups of unpolarized epithelial cells form microlumens, which subsequently participate in the formation of tubes where branching is not entirely stereotypical (Hogan and Kolodziej, 2002). Whereas the first process is relatively well understood, the latter is not.

Tubulogenesis involves a series of dynamic and interdependent cellular processes, including cytoskeletal reorganization, assembly of intercellular junctional complexes, and cell polarization. Rho-GTPases are molecular switches that control such complex processes. For example, Cdc42, which is one of the most studied Rho-GTPase family members, is a master regulator of cytoskeletal dynamics and cell polarity – a function which is

evolutionary conserved from yeast to mammals (Etienne-Manneville, 2004).

Recently, Cdc42 was demonstrated to control lumen formation in three-dimensional (3D) organotypic cultures of MDCK and Caco-2 cells by controlling apical segregation of phosphoinositides and spindle orientation during cell division, respectively (Jaffe et al., 2008; Martin-Belmonte et al., 2007). Whether Cdc42 controls lumen formation in vivo in a similar manner remains unclear.

The pancreas is a glandular organ where the tubular network interconnects the acinar cells and enables coordinated transport of digestive enzymes into the duodenum. Organogenesis of the pancreas begins with the evagination of the dorsal and ventral anlagen from the foregut endoderm. In mice, this event starts at embryonic day (E) 8.5. The pancreatic epithelium is in contact with various sources of mesodermally-derived tissues whose signals are crucial for pancreatic growth and differentiation (Gittes, 2008). Pancreatic and duodenal homeobox 1 (Pdx1) expressing multipotent pancreatic progenitors give rise to all epithelial cells of the adult pancreas, including duct, acinar, and endocrine cells (Gu et al., 2002).

Here, we have used the mouse pancreas to address two fundamentally important questions in developmental biology, namely the molecular control of mammalian organ asymmetry and tubulogenesis in vivo and the interplay between tube formation and cell fate decisions during organogenesis. First, we show that tube formation starts

at E11.5 by the initiation of scattered microlumens throughout the epithelium. These lumens expand by spreading of cell polarization, and not by sprouting, followed by fusion of lumens and their rearrangement into an interconnected tubular system. Second, by ablating Cdc42 at different time points during pancreas development, we demonstrate that Cdc42 is required for microlumen formation and subsequently for maintenance of a polarized tubular phenotype. Third, the failure to organize pancreatic epithelial progenitors into tubes cause a dramatic upregulation of acinar cell differentiation at the expense of duct and endocrine cell differentiation. Finally, we show that this is non-cell-autonomously caused by changes in epithelial cell-extra cellular matrix (ECM) interactions.

## RESULTS

### Formation of tubes during pancreas development

To understand the basis for pancreatic tubulogenesis, we first characterized the establishment of epithelial cell polarity and tube formation during pancreas development. Mucin1 (Muc1) is an O-glycosylated transmembrane protein expressed on the apical surface of many epithelia, including the pancreas (Cano et al., 2004). Thus, Muc1 was used as an apical marker, whereas the cell-cell adhesion protein E-cadherin (Ecad) and the basement membrane protein laminin (Lam) were used as lateral and basal markers, respectively (Figure 1A-E). To image the luminal system three-dimensionally,

whole-mount Muc1 immunofluorescence analysis was carried out (Figure 2A-F). Except for a stunted opening into the duodenum, the E10.5 dorsal pancreatic bud is multilayered, consisting of epithelial cells that lack apico-basal cell polarity. Furthermore, the epithelium lacks luminal structures and is surrounded by laminin (Figure 1A). The first sign of lumen formation occurs at E11.5 with the stochastic appearance of microlumens scattered throughout the epithelium (Figure 1B and 2A, D; arrowhead indicates microlumen). The microlumens are made up of clusters of epithelial cells with a common apical surface facing the lumen. Subsequently, the microlumens expand by inducing apical cell polarity in neighboring epithelial cells resulting in a complex network of independently organized luminal structures (Figure S1A, B). At E12.5 the lumens coalesce into a complex continuous luminal network within the multilayered epithelium (Figure 1C and 2B, E). Notably, at this point no tubes have formed. However, between E13.5 and E15.5 the luminal network remodels and matures into a tubular network, i.e. this is the stage when the first tubes consisting of a monolayered fully polarized epithelium surrounded by a basal lamina forms (Figure 1D, E; 2C, F and S2). This process can be visualized by changes in the organization of basal lamina components, including laminin. Whereas laminin is distributed mainly on the periphery of the early pancreatic bud, it covers the entire tubular monolayered epithelium at later time points (Figure S2). Moreover, ultrastructural analysis at E15.5 confirmed

the hallmarks of a fully polarized tubular epithelium, including cell-cell junctions and protruding microvilli on the apical surface (Figure 1F).

### **Cdc42 is required for tubulogenesis during pancreas development**

The Par-aPKC complex is regulated by Cdc42 and plays a critical role in cell polarity initiation and maintenance. Binding of Cdc42-GTP activates the Par/aPKC complex and the phosphorylated form of aPKC (p-aPKC) was used as a marker to identify the activated form of aPKC (Wu et al., 2007). At E11.5, p-aPKC was specifically distributed along the apical surface of microlumens together with characteristic apical markers, including ZO-1, Par6, Muc1, and crumbs3 (Figure 3A,B and S3A). In situ hybridization analysis demonstrated that *Cdc42* mRNA is ubiquitously expressed in the entire pancreas at all development stages analyzed (Figure S3B).

To specifically ablate Cdc42 during pancreas development *floxed Cdc42* mice were intercrossed with *Pdx1-cre* mice (Gu et al., 2002; Wu et al., 2006). From here on *Cdc42<sup>fl/fl</sup>* or *Cdc42<sup>fl/+</sup>* mice are referred as wildtype (WT) mice, whereas *Cdc42<sup>fl/+</sup>; Pdx1-cre* and *Cdc42<sup>fl/fl</sup>; Pdx1-cre* mice are referred as Cdc42 het and Cdc42 KO mice, respectively. Cdc42 het were indistinguishable from WT controls (data not shown). Analysis of the recombination efficiency of the *Pdx1-cre* line using the *R26R LacZ* reporter line demonstrated undetectable recombination at E10.5, whereas approximately 90-95% of the

epithelial cells underwent cre-mediated recombination at E11.5. Consistently, cre efficiently ablated the Cdc42 protein (Figure S3C and D). As a consequence the first phenotype was apparent at E11.5. In contrast to the WT epithelium where apical polarity is induced concomitant with microlumen formation, apical membrane proteins, e.g. Muc1, remained intracellular within the Cdc42 KO epithelium (compare Figure 1B with B' and S4A with S4A'). Furthermore, Q-PCR analysis revealed a two-fold upregulation of *Muc1* mRNA expression, which most likely is due to an increased number of Muc1<sup>+</sup> cells (Figure S4D). In contrast, E-cadherin and laminin showed normal distribution (Figure 1B'-E'), suggesting that Cdc42 ablation did not affect the formation of the lateral and basal surfaces. The unpolarized Cdc42 KO epithelia failed to retain its integrity and became fragmented into epithelial cords. Cell proliferation gradually transformed these structures into large cellular aggregates lacking tubular structures (Figure 1C'-E'). Whole-mount immunofluorescence analysis of Muc1 in Cdc42 KO E11.5 to E13.5 pancreas, confirmed the lack of tubes, as well as the change in Muc1 distribution (Figure 2 A'-C'). Transmission electron microscopy (TEM) analysis at E15.5 corroborated the failure to establish tubes (Figure 1F'). Thus, Cdc42 is essential for tubulogenesis in the developing pancreas.

### **Cdc42 is required for multicellular apical polarization**

Careful examination of microlumen

formation revealed that induction of apical cell polarity appears to initially involve only one cell. At E11.5, Muc1 is confined to a distinct vesicular compartment close to the plasma membrane (Figure S4A). This intracellular vesicular compartment may represent the same secretory vesicles delivered to the de novo apical membrane concomitant with formation of primitive cell-cell junctions (Figure S4B and C). Importantly, these events are only seen at E11.5. Altogether, these results suggest that microlumens are initiated by one cell that upon a given signal induces targeting of secretory vesicles containing apical membrane proteins to the presumptive apical domain. Shortly thereafter neighboring cells undergo apical polarization resulting in a shared apical domain facing a lumen.

In the absence of Cdc42, characteristic apical membrane proteins and membrane-associated proteins, including Muc1, ZO-1, Par6, crumbs3, and cortical F-actin, are primarily confined to luminal structures within cells (Figure 3A-C). Careful TEM analysis revealed that these lumens (from here on referred to as “autocellular” lumens) are in fact in direct contact with the cell surface via ZO-1<sup>+</sup> and claudin3<sup>+</sup>, “autocellular” tight junction-like junctions (Figure S1C, D and S5). Intercellular lumens between two cells also form, but less frequently (Figure 3C and S1E, F). The apical membrane phenotype of both the “autocellular” and intercellular luminal surfaces is reinforced by the appearance of microvilli-like structures (Figure S1C-F and H). Finally, Cdc42

ablation does not affect the intracellular distribution of proteins involved in the general vesicular targeting machinery, such as VAP-A (VAMP associated protein A) (Figure S4E). Based on these findings, Cdc42 is not required for apical membrane biogenesis or for tight junction formation. However, whether the apical domain and tight junctions in the absence of Cdc42 are fully mature and functional remains to be determined. In summary, Cdc42 is necessary for maintaining an apical surface facing the outside of cells, and to establish multicellular (> 2 cells) microlumens with shared apical surfaces.

### **Cdc42 is required for maintenance of tubes**

Ablating Cdc42 during the earliest stages of pancreas development failed to address whether Cdc42, in addition to its role in microlumen formation, plays a role in maintaining cell polarity in the tubular epithelium. To address this question, we used a tamoxifen (TM) inducible model (*Pdx1-cre ER<sup>TM</sup>* mice) for timed ablation of Cdc42 within the pancreatic epithelium (Gu et al., 2002). By intercrossing the *R26R LacZ* reporter line (Soriano, 1999) with *Pdx1-cre ER<sup>TM</sup>* mice recombined cells became traceable by their expression of beta-galactosidase ( $\beta$ Gal). To address the role of Cdc42 in maintenance of tubes *Cdc42<sup>fl/+</sup>; Pdx1-cre ER<sup>TM</sup>; R26R* and *Cdc42<sup>fl/fl</sup>; Pdx1-cre ER<sup>TM</sup>; R26R* mice were generated. Cdc42 was ablated by a single tamoxifen pulse at E12.5 followed by analysis at E15.5. Thus, at the time of tamoxifen induction these cells were

polarized and confined to the primitive tubular network. This mosaic system (*Cdc42<sup>fl/fl</sup>; Pdx1-cre ER<sup>TM</sup>*) resulted in a recombination efficiency of 16% (data not shown), which is not sufficient to block tubulogenesis and alter the overall tissue architecture (Figure S6). In control samples, all  $\beta$ Gal<sup>+</sup> cells were randomly distributed within tubes as fully polarized epithelial cells with an apical surface enriched with Muc1, claudin3, Par6 and cortical F-actin (Figure 4A-F). In the mosaic Cdc42 KO model  $\beta$ Gal<sup>+</sup> cells were found both within and outside the tubular epithelium. However, the few  $\beta$ Gal<sup>+</sup> Cdc42 KO cells that were found interspersed between WT cells within tubes failed to maintain apical cell polarity, as demonstrated by failure to maintain Muc1, Par6, and cortical F-actin on the apical side (Figure 4A', C' and E'). Furthermore, less claudin3 were found at tight junctions of  $\beta$ Gal<sup>+</sup> cells (Figure 4 F, F'). Interestingly, basal polarity as detected by laminin deposition was unaffected (Figure 4 G, G'). Delaminating  $\beta$ Gal<sup>+</sup> Cdc42 KO cells clustered into epithelial aggregates without an apical surface (Figure 4 B', D'). Intracellular accumulation of apical markers, such as Muc1, and loss of cortical F-actin were observed (Figure 4B', D'). Loss of apical polarity resulted in replacement of the apical membrane by lateral membrane, as evidenced by expression of the lateral surface marker, E-cadherin (Figure S7). In conclusion, Cdc42 not only plays a cell-autonomous role in microlumen formation, but also in maintenance of apical polarity in fully polarized tubular epithelial cells.

### **aPKC is required for lumen coalescence into a continuous tubular network**

Q-PCR analysis showed that both the *aPKC $\zeta$*  and *aPKC $\iota$*  isoforms are expressed in the developing pancreas (Figure S4D). The activated form of aPKC, p-aPKC, is expressed on the apical membrane throughout the pancreatic lumens and tubes until E13.5 (Figure S8A-D). Ablation of Cdc42 resulted in undetectable levels of p-aPKC within the epithelium from E11.5 onwards, whereas expression of p-aPKC within blood vessels was unaffected (Figure S8A'-D'). To test the hypothesis that Cdc42 controls microlumen formation through aPKC activation we examined whether blocking aPKC activation would mimic the Cdc42 KO phenotype. For this purpose, we used a two-dimensional (2D) explants culture system that provides a simple and effective way to analyze tubulogenesis in vitro (Percival and Slack, 1999). Treatment of the explants with the myristoylated substrate of aPKC $\zeta$  (aPKC-PS) effectively inhibited the activation of aPKC, whereas expression of the protein remained unaffected (Figure S9A, B) (Nunbhakdi-Craig et al., 2002). Untreated controls formed a continuous tubular network, whereas Cdc42 KO explants failed to form tubes due to their lack of apical cell polarity (Figure S9C). aPKC-PS-treated WT explants failed to generate a continuous tubular network. Instead, the epithelium remained compact with large aggregates of epithelial cells (Figure S9C). However, in contrast to the intracellular accumulation of Mucl in the Cdc42 KO epithelial cells, apical cell

polarity appeared unaffected in aPKC-PS-treated epithelial aggregates (Figure S9C). These results show that aPKC plays a crucial role in lumen coalescence into a continuous tubular network in vitro. This observation is consistent with the multiple lumen phenotype in the intestine of aPKC mutants in Zebrafish (Horne-Badovinac et al., 2001). Altogether, these results suggest that Cdc42 controls tubulogenesis in vivo at several levels, and that aPKC activation through Par6 represents one of several Cdc42-controlled pathways involved in tubulogenesis.

### **Inhibition of Rho kinase restores tube formation in the Cdc42 KO epithelium**

Cdc42 acts in several ways to establish a functional and mature apical surface, e.g. by interacting with the master polarity complex proteins Par3, Par6 and aPKC (Bryant and Mostov, 2008). Par3 interaction with the Par6-aPKC complex is indispensable for apical domain development (Horikoshi et al., 2009). Therefore, failure to establish a common apical domain in the absence of Cdc42 may be attributed to disturbed interaction of Par3 with the Par6/aPKC complex. Recently, it was demonstrated that Rho kinase (ROCK) also controls formation of the Par3/Par6/aPKC complex by phosphorylation of Par3, which prevents its interaction with Par6 and aPKC (Nakayama et al., 2008). To test if blocking ROCK activity could restore apical polarity and tubulogenesis in the Cdc42 KO epithelium, WT and Cdc42 KO explants were incubated with the ROCK inhibitor, Y27632. Pharmacological

inhibition of Rho kinase activity in vitro restored tube formation in the Cdc42 KO epithelium (Figure S10). Further studies are required to fully understand this intriguing result.

### **Perturbed “tip-trunk” organization alters the proportion and distribution of Cpa<sup>+</sup> and Ptf1a<sup>+</sup> progenitors**

Between E13.5 to E15.5, lineage commitment of multipotent Pdx1<sup>+</sup> pancreatic progenitors towards exocrine and endocrine lineages is active (Gittes, 2008; Jorgensen et al., 2007). Notably, these lineages appear at distinct anatomical positions within the developing tubular network. All peripheral epithelial cells, including “tip cells” and acinar progenitors (Zhou et al., 2007), are exposed to ECM proteins, including laminin, and mesenchymal cells throughout development (Figures S2A and S11A). In contrast, before formation of a monolayered tubular epithelium, the central parts (trunk) of the epithelium consisting of endocrine and ductal progenitors are sparsely exposed to ECM and mesenchymal cells. The failure to organize Cdc42 KO multipotent pancreatic progenitors into tubes provides a model for addressing the importance of tissue/microenvironment asymmetry in cell specification.

Ablation of Cdc42 had no impact on the expression of Pdx1, Nkx6.1, and Sox9 in Pdx1<sup>+</sup> multipotent progenitors up until E13.5 (Figure S11B). A subpopulation of the multipotent progenitors confined to the tips of the tubular network, “tip cells”, express carboxypeptidase A1 (Cpa1),

along with Pdx1, Ptf1a and cMyc until E14 (Zhou et al., 2007). The fact that the Cdc42 KO pancreatic epithelium lacked distinct “tip-trunk” structures (Figure 5A, B and A', B') led to a randomized distribution of “tip cell” markers, such as Cpa1 and Ptf1a. Although the total number of epithelial cells was unaffected, the relative number of Cpa1<sup>+</sup> and Ptf1a<sup>+</sup> progenitors increased at E13.5 (Figure 5 C, D; data not shown). In addition, cleaved Caspase3 stainings showed no significant difference in the frequency of apoptotic cells between the WT and Cdc42 KO epithelium ( $0.56\% \pm 0.04$  (WT) and  $0.41\% \pm 0.11$  (KO)). Thus, Cdc42-controlled tissue/microenvironment asymmetry is required for regulating the distribution and number of Cpa1<sup>+</sup> and Ptf1a<sup>+</sup> pancreatic progenitors.

### **Cdc42 ablation results in increased acinar differentiation at the expense of endocrine commitment**

Quantification of *Ngn3* mRNA expression demonstrated a significant reduction in Cdc42 KO samples at E14.5 (Figure 5G). Consistently, immunofluorescence staining of Ngn3 at E15.5 showed significantly fewer Ngn3 positive cells in the KO epithelium (Figure 5E, E'). In line with this observation, a dramatic reduction of insulin and glucagon expressing cells was observed at E15.5 (Figure 5F, F', and H). These results show that differentiation toward endocrine cell lineages is severely compromised upon Cdc42-deficiency.

In contrast, expression of *Ptf1a*, *elastase* and *amylase* mRNAs and amylase and Cpa1 proteins increased, suggesting that

acinar cell differentiation increased in the absence of Cdc42 (Figure 6A, B, A', B', D-F). In the WT pancreas Sox9 was distributed throughout the branching tubular tree, except for within the terminal acinar structures (Seymour et al., 2007). In the E15.5 Cdc42 KO epithelium very few Sox9<sup>+</sup> duct cells were found and they were randomly distributed within the epithelial aggregates (Figure 6C, C'). At E17.5, the phenotype was comparable to E15.5 with many acinar cells, but few endocrine and duct cells (Figure S12B). Postnatally, the Cdc42 KO animals were growth retarded and developed cysts in the stomach and a distended duodenum (Figure S12A). Moreover, acinar cysts developed within the pancreas. The majority of these cysts were multicellular consisting of polarized cells with apical junctions. However, large cysts from single cells were also observed (Figure S12B, C, and data not shown). In summary, Cdc42 ablation results in increased acinar cell differentiation at the expense of endocrine and duct cell differentiation. This indicates that Cdc42 is required for proper specification of multipotent pancreatic progenitors into acinar, duct and endocrine cells.

In vitro culture of the embryonic pancreas in the absence of mesenchyme suppresses cell proliferation and acinar differentiation, but enhances endocrine specification. Therefore, it was proposed that multipotent progenitors choose islet fate by default (Duvillie et al., 2006; Gittes et al., 1996). To address if Cdc42 controls endocrine cell specification in a cell-autonomous or non-cell-autonomous manner, WT and

Cdc42 KO E11.5 intact pancreatic buds (Epi + Mes) and epithelium devoid of mesenchyme (Epi - Mes) were cultured as explants for 7 days. The WT Epi - Mes explants preferentially differentiated towards endocrine lineages, whereas Epi + Mes explants generated endocrine and exocrine lineages comparable to in vivo conditions (Figure 7A-D). Consistent with the observed reduction of endocrine cells in vivo, the relative number of endocrine cells was reduced in Cdc42 KO Epi + Mes explants (compare Figure 7A, B with 7A', B' and 7H). Surprisingly, in the absence of the mesenchyme the WT and Cdc42 KO explants generated the same number of insulin and glucagon expressing cells (compare Figure 7C, D with 7 C',D' and 7I). All insulin<sup>+</sup> cells (independent of genotype) co-expressed Pdx1, indicating that they represent secondary transition insulin<sup>+</sup> cells (Figure S13). Altogether, these findings rule out that Cdc42 controls endocrine cell differentiation in a cell-autonomous manner, and suggest that altered tissue architecture/microenvironment is responsible for Cdc42 KO-induced changes in cell fate specification.

### **Laminin-1 promotes acinar cell lineage commitment in multipotent pancreatic progenitors**

The mesenchyme produces and secretes ECM components, such as laminin-1. Epithelial cells in contact with laminin-1 differentiate into acini and inhibiting laminin-1 translation with antisense morpholinos blocked exocrine cell

differentiation, whereas endocrine cell differentiation was unaffected (Crisera et al., 2000; Li et al., 2004). Consistent with these observations is the demonstration that expression of laminin and acinar cell differentiation are compromised during in vitro culture of mesenchyme depleted pancreatic explants (Epi - Mes) (Figure S13) (Duvillie et al., 2006). Altogether, these results support a pro-acinar cell specification role of laminin-1. Fragmentation of the Cdc42-deficient pancreatic epithelium resulted in increased mixture between mesenchymal and epithelial cells (Figure 7E and E'). As a consequence, the majority of the Cdc42 KO multipotent pancreatic progenitors were in direct contact with laminin and mesenchymal cells throughout development (compare Figure 7F, G with F', G'). To test whether laminin-1 act as an pro-acinar factor within the Cdc42 KO epithelium, E11.5 WT and Cdc42 KO pancreatic explants were cultured in the absence or presence of functional blocking antibodies against laminin alpha 1 chain (Sorokin et al., 1992). Comparing untreated and treated WT explants showed a trend towards reduced acinar differentiation in the presence of the laminin antibody. Importantly, blocking laminin-1 function in Cdc42 KO explants restored the number of acinar cells to WT levels, whereas it failed to rescue endocrine cell differentiation (Figure 7J and S14).

### **Tissue architecture/microenvironment controls endocrine cell specification**

Comparing the effect of blocking aPKC

activity on tissue architecture with the effects seen in the mosaic and complete Cdc42 KO models revealed an intermediate phenotype (Figures 1, S6, and S9). In this model acinar differentiation was unaffected, whereas a two-fold reduction in endocrine differentiation was observed (Figure S9D).

Notch signaling is the central pathway controlling differentiation decisions in the developing pancreas. Q-PCR analysis revealed no change in the expression of Notch receptors and ligands at E14.5. However, Cdc42 ablation resulted in a slight upregulation of *Hes1* mRNA (Figure S15A). To test the functionality of Notch signaling, both WT and Cdc42 KO pancreas explants were treated with a gamma secretase inhibitor (DAPT). As expected, treating WT explants with DAPT resulted in a significant increase in the number of endocrine cells. In contrast, DAPT treatment failed to rescue endocrine cell fate specification in the Cdc42 KO explants (Figure S15B). These findings underpin the importance of the tubular network in providing a microenvironment permissive for Notch-mediated specification of endocrine cell types.

## **DISCUSSION**

Most, if not all, morphogenetic processes involve alterations in cell polarity. However, how polarity is established and remodeled during morphogenesis is poorly understood. In particular, in pseudo-stratified or multilayered epithelia, such as the pancreas, salivary glands and

mammary gland, regulation of cell polarity and biogenesis of the apical membrane during tissue polarity and tube formation is more complex compared to simple epithelia. Tubulogenesis often coincides with cell lineage specification during organ development. Hence, an elementary question is whether these two processes are independently controlled, or whether proper cell specification depends on formation of tubes.

### **Acquiring apical cell polarity initiates tubulogenesis in multilayered epithelia**

Two basic mechanisms of lumen formation in unpolarized cells have been proposed, i.e. cord hollowing and cavitation (Chung and Andrew, 2008). Characterization of the different stages of pancreatic tubulogenesis identified at least three critical events. First, at a distinct time point, E11.5, microlumens form throughout the epithelium. The initial event in microlumen genesis involves the induction of apical cell polarity within single cells. Complete polarization of single cells has previously been reported in intestinal epithelial cells (Baas et al., 2004). Thereafter, groups of fully polarized cells assemble into microlumens. Notably, apoptosis was not observed during microlumen formation. Thus, the initial luminal structures appear to form through a hollowing principle. Second, preexisting microlumens expand into a complex network of independently organized luminal structures. The wide variety of shapes of lumens suggests that no stereotypical program controls expansion of the lumens. Notably, at

this point all lumens are confined to a multilayered epithelium, i.e. no tubes have formed. Third, concomitant with the fusion of lumens the first tubes form through complex epithelial cell rearrangement. Soon thereafter the tubes mature into a continuous monolayered polarized tubular epithelial network (schematic Figure 3D and S16).

Ablation of Cdc42 in the developing pancreas results in complete failure to form tubes. Based on our findings we propose a new model for how tubes form within multilayered unpolarized epithelium and how this process is controlled by Cdc42.

Regulation of cell polarity occurs at three major levels. Intrinsic mechanisms include the sorting of membrane proteins into different post-Golgi or endosomal vesicles and their delivery to different membrane domains for membrane fusion (Mellman and Nelson, 2008). The identity of plasma membrane domains are controlled by protein complexes (the Par, crumbs, and scribble complexes) localized to the plasma membrane (Bilder et al., 2003; Tanentzapf and Tepass, 2003). Finally, extrinsic cues mediated by cell adhesion to cells and ECM control the orientation of cell polarity (Yu et al., 2005). Most probably, all three layers of regulation are required to establish proper tissue/organ polarity.

We show that Cdc42 ablation does not block delivery of apical membrane proteins to the surface, indicating that post-Golgi transport is not blocked. Instead, microlumen formation fails because Cdc42 is required for inducing apical

cell polarity and tight junction-coupling with neighboring cells – a prerequisite for establishing shared lumens of more than two cells. This suggests that Cdc42 may be required for signaling to its neighboring cells to initiate apical cell polarity and tight junction coupling, or for receiving such signals within neighboring cells, or for both. We can only speculate on the nature of such signal, but it seems reasonable to assume that it may involve communication via the junctional complex, more specifically the tight junctions. This tentative scenario is in agreement with a recent study showing the role of Cdc42 in continuous junctional spreading in the developing *Drosophila notum* (Georgiou et al., 2008). Finally, conditional ablation of Cdc42 showed that Cdc42 is not only required for microlumen formation, but also for maintaining a polarized tubular phenotype by sustaining an apical surface in a cell autonomous manner.

### **Tubes are necessary for proper cell fate specification**

Signals that control tubulogenesis also control cell specification. For example, signaling pathways acting as chemoattractants during epithelial branching, e.g. Bnl/Fgf signaling, also determines whether a tracheal epithelial cell becomes a tip or stalk cell (Ghabrial and Krasnow, 2006). Correspondingly, maintenance of a tip cell phenotype is regulated by FGF signaling in the mammary gland (Lu et al., 2008).

Detailed comparison between the complete and mosaic ablation of Cdc42 and the

inhibition of aPKC activity demonstrates that pancreatic cell fate specification requires tubes to ensure that multipotent Pdx1<sup>+</sup> pancreatic progenitors are confined to distinct microenvironments. Pancreatic progenitors in the periphery of the branching epithelium are continuously exposed to basal lamina components, e.g. laminins, and mesenchymal cells, whereas the more centrally localized progenitors primarily interact with one another (until E13.5). It is only later when tubes are beginning to form (E13.5 to 15.5) that the latter cells become exposed to basement membrane components and mesenchymal cells. Hence, the consequence of ablating Cdc42 in all pancreatic progenitors is that virtually all progenitors become exposed to the same environment as the peripheral progenitors. Consistently, the progenitors maintain expression of Ptf1a and differentiate into acinar cells, the normal fate of peripheral “tip cell” progenitors (Zhou et al., 2007). As a consequence endocrine and duct cell differentiation become compromised. Interestingly, blocking aPKC activity also resulted in reduced endocrine cell specification, but acinar specification was unaffected. Limited invasion by mesenchymal cells and ECM (laminin) may explain the lack of effect on acinar differentiation, whereas failure to generate continuous tubes most likely explains the endocrine phenotype. Importantly, *in vitro* explant experiments demonstrated that Cdc42 does not affect endocrine lineages directly as they were as capable as WT epithelium to differentiate into endocrine cells. In conclusion, these results provide an explanation for how a

direct role of Cdc42 in tissue architecture secondarily specifies microenvironments permissive for specification of multipotent Pdx1<sup>+</sup> pancreatic progenitors.

Finally, current attempts to develop protocols for generating insulin-producing beta cells from various stem/progenitor cell sources are based on how pancreatic beta cells normally develop in vivo. So far, it has been unclear if and how the tissue architecture/microenvironment influences cell specification during beta cell development. Consequently most in vitro differentiation protocols do not take these issues into consideration. Our data demonstrates that pancreatic cell fate specification requires tubes. Tubulogenesis ensures confinement of multipotent Pdx1<sup>+</sup> pancreatic progenitors to distinct microenvironments, which is a prerequisite for appropriate cell fate determination. This emphasizes the significance of understanding the underlying molecular principles for how distinct microenvironments along the “tip-trunk” axis control pancreatic cell fate choices in vivo. Filling in these gaps will most likely provide new strategies for developing robust and efficient protocols to generate beta cells from stem/progenitor cells in vitro.

## EXPERIMENTAL PROCEDURES

### Mice

Homozygous *Cdc42 fl/fl* mice (*loxP* sites flanking exon 2) (Wu et al., 2006) were intercrossed with *Pdx1<sup>cre/cre</sup> Cdc42 fl/+* mice (Gu et al., 2002) to obtain Cdc42 KO

embryos (*Pdx1<sup>cre/cdc42 fl/fl</sup>*). Littermates possessing one or two *loxP* flanked (floxed) alleles without cre were used as wildtype controls (WT). The day of vaginal plug was counted as E0.5. For the inducible model of *Pdx1 cre-ER<sup>TM</sup>* (Gu et al., 2002) the same breeding strategy was followed, except for that *R26RLacZ* mice (Soriano, 1999) were included. Tamoxifen dissolved in corn oil (1.5 mg/animal) was injected intraperitoneally in pregnant females. All animal work was carried out in accordance with the local ethics committee for animal research.

### Immunofluorescence stainings and Microscopy

Embryonic pancreases were fixed in 4% paraformaldehyde for 3-4 hrs at 4°C, cryoprotected in 30% sucrose, embedded in Tissue-Tek and sectioned. Sections were incubated with primary antibodies (Supplementary table 1), overnight at 4°C in 5% skimmed milk or in 5% normal donkey serum. Secondary antibodies were used according to the manufacturer’s protocol (Jacksons immunoresearch and Molecular probes). Immunostainings were analyzed with Zeiss axioplan2 or LSM510 laser scanning microscope. Whole-mount immunofluorescence was done as previously described (Jorgensen et al., 2007). Imaris (Bit-plane) was used to analyze confocal images and to create 3D reconstructions in Maximum Intensity Projection mode.

### Transmission Electron Microscopy

The pancreas tissue was fixed overnight in

2.5% glutaraldehyde in 0.1M Phosphate buffer and post-fixed for 1hour with 1% osmium tetroxide at 4°C. After dehydration and standard embedding in Agar 100, 50nm ultrathin sections were cut on a Leica UCT ultra microtome (Leica Microsystems), post-stained with uranyl acetate and lead citrate and viewed in a JEOL JEM 1230 electron microscope.

### **Explant cultures, inhibition assays and morphometry**

E11.5 dorsal pancreas (DP) was dissected out and cultured on filter inserts (0.4 µm, Millipore) for 7 days as previously described (Edsbagge et al., 2005). For the Epi – Mes explants, the epithelium was isolated from the DP by mechanically removing the mesenchyme under a dissection microscope and cultured for 7 days. The intact dorsal pancreas (Epi + Mes) was used as controls. The day of harvest, D=0.

For the aPKC and laminin-1 blocking assays, E11.5 dorsal pancreas was cultured on fibronectin coated coverslips for 7 days (Percival and Slack, 1999). In the aPKC inhibition studies, myristoylated substrate of aPKC $\zeta$  (aPKC-PS, calbiochem) at 40µg/ml was added on day 1, 3 and 5. Control experiments showed that treatment of pancreatic explants with aPKC-PS at 40 µg/ml resulted in complete loss of activated aPKC (Figure S9A, B).

To block laminin-1 function, pancreatic explants were incubated with functional-blocking antibodies against laminin-1 alpha chain (200 µg/ml) on day 1, 3 and 5.

The explants were fixed in 4% PFA, stained as whole-mounts and analyzed by confocal microscopy. Volume measurements were made on the 3D reconstructed images (Imaris). Statistical significance was tested with unpaired, two-tailed student's t-test and the differences were considered to be statistically significant when  $p < 0.05$ . The values in the histograms represent mean  $\pm$  SEM.

### **Quantitative PCR**

RNA extraction from E14.5 pancreas was done according to manufacturers protocol (Qiagen). cDNA was prepared using Superscript II (Invitrogen) with random hexamers. Real time PCR was measured in ABI PRISM 7900 using SYBR Green. Primer sequences are presented in supplemental table 2.

### **ACKNOWLEDGEMENTS**

We thank M. Durbeej, B. Margolis, S. Ohno, C. Wright and the Beta Cell Biology Consortium for providing antibodies; G. Gu and P. Serup for providing Cre lines; I. Artner P. Nyeng and Y. Fischer for comments on the manuscript, V.F. Gregoire for quantifying mitotic index, J. Ameri for QPCR, M. Magnusson and C. Ekenstierna for mouse breeding, U. Häcker for helpful discussions and R. Wallen for the TEM analysis. This work was supported by the Swedish Research Council, Stem Cell Center Lund University, Swedish Foundation for Strategic Research and NIH Beta Cell Biology Consortium.

### **REFERENCES**

- Baas, A.F., Kuipers, J., van der Wel, N.N., Batlle, E., Koerten, H.K., Peters, P.J., and Clevers, H.C. (2004). Complete polarization of single intestinal epithelial cells upon activation of LKB1 by STRAD. *Cell* *116*, 457-466.
- Bilder, D., Schober, M., and Perrimon, N. (2003). Integrated activity of PDZ protein complexes regulates epithelial polarity. *Nat Cell Biol* *5*, 53-58.
- Bryant, D.M., and Mostov, K.E. (2008). From cells to organs: building polarized tissue. *Nat Rev Mol Cell Biol* *9*, 887-901.
- Cano, D.A., Murcia, N.S., Pazour, G.J., and Hebrok, M. (2004). Orpk mouse model of polycystic kidney disease reveals essential role of primary cilia in pancreatic tissue organization. *Development* *131*, 3457-3467.
- Chung, S., and Andrew, D.J. (2008). The formation of epithelial tubes. *J Cell Sci* *121*, 3501-3504.
- Crisera, C.A., Kadison, A.S., Breslow, G.D., Maldonado, T.S., Longaker, M.T., and Gittes, G.K. (2000). Expression and role of laminin-1 in mouse pancreatic organogenesis. *Diabetes* *49*, 936-944.
- Duvillie, B., Attali, M., Bounacer, A., Ravassard, P., Basmaciogullari, A., and Scharfmann, R. (2006). The mesenchyme controls the timing of pancreatic beta-cell differentiation. *Diabetes* *55*, 582-589.
- Edsbagge, J., Johansson, J.K., Esni, F., Luo, Y., Radice, G.L., and Semb, H. (2005). Vascular function and sphingosine-1-phosphate regulate development of the dorsal pancreatic mesenchyme. *Development* *132*, 1085-1092.
- Etienne-Manneville, S. (2004). Cdc42-
- the centre of polarity. *J Cell Sci* *117*, 1291-1300.
- Georgiou, M., Marinari, E., Burden, J., and Baum, B. (2008). Cdc42, Par6, and aPKC regulate Arp2/3-mediated endocytosis to control local adherens junction stability. *Curr Biol* *18*, 1631-1638.
- Ghabrial, A.S., and Krasnow, M.A. (2006). Social interactions among epithelial cells during tracheal branching morphogenesis. *Nature* *441*, 746-749.
- Gittes, G.K. (2008). Developmental biology of the pancreas: A comprehensive review. *Dev Biol*.
- Gittes, G.K., Galante, P.E., Hanahan, D., Rutter, W.J., and Debase, H.T. (1996). Lineage-specific morphogenesis in the developing pancreas: role of mesenchymal factors. *Development* *122*, 439-447.
- Gu, G., Dubauskaite, J., and Melton, D.A. (2002). Direct evidence for the pancreatic lineage: NGN3<sup>+</sup> cells are islet progenitors and are distinct from duct progenitors. *Development* *129*, 2447-2457.
- Hogan, B.L., and Kolodziej, P.A. (2002). Organogenesis: molecular mechanisms of tubulogenesis. *Nat Rev Genet* *3*, 513-523.
- Horikoshi, Y., Suzuki, A., Yamanaka, T., Sasaki, K., Mizuno, K., Sawada, H., Yonemura, S., and Ohno, S. (2009). Interaction between PAR-3 and the aPKC-PAR-6 complex is indispensable for apical domain development of epithelial cells. *J Cell Sci* *122*, 1595-1606.
- Horne-Badovinac, S., Lin, D., Waldron, S., Schwarz, M., Mbamalu, G., Pawson, T., Jan, Y., Stainier, D.Y., and Abdelilah-Seyfried, S. (2001). Positional cloning of heart and soul reveals multiple roles for

- PKC lambda in zebrafish organogenesis. *Curr Biol* *11*, 1492-1502.
- Jaffe, A.B., Kaji, N., Durgan, J., and Hall, A. (2008). Cdc42 controls spindle orientation to position the apical surface during epithelial morphogenesis. *J Cell Biol* *183*, 625-633.
- Jorgensen, M.C., Ahnfelt-Ronne, J., Hald, J., Madsen, O.D., Serup, P., and Hecksher-Sorensen, J. (2007). An illustrated review of early pancreas development in the mouse. *Endocr Rev* *28*, 685-705.
- Li, Z., Manna, P., Kobayashi, H., Spilde, T., Bhatia, A., Preuett, B., Prasad, K., Hembree, M., and Gittes, G.K. (2004). Multifaceted pancreatic mesenchymal control of epithelial lineage selection. *Dev Biol* *269*, 252-263.
- Lu, P., Ewald, A.J., Martin, G.R., and Werb, Z. (2008). Genetic mosaic analysis reveals FGF receptor 2 function in terminal end buds during mammary gland branching morphogenesis. *Dev Biol* *321*, 77-87.
- Martin-Belmonte, F., Gassama, A., Datta, A., Yu, W., Rescher, U., Gerke, V., and Mostov, K. (2007). PTEN-mediated apical segregation of phosphoinositides controls epithelial morphogenesis through Cdc42. *Cell* *128*, 383-397.
- Mellman, I., and Nelson, W.J. (2008). Coordinated protein sorting, targeting and distribution in polarized cells. *Nat Rev Mol Cell Biol* *9*, 833-845.
- Metzger, R.J., Klein, O.D., Martin, G.R., and Krasnow, M.A. (2008). The branching programme of mouse lung development. *Nature* *453*, 745-750.
- Nakayama, M., Goto, T.M., Sugimoto, M., Nishimura, T., Shinagawa, T., Ohno, S., Amano, M., and Kaibuchi, K. (2008). Rho-kinase phosphorylates PAR-3 and disrupts PAR complex formation. *Dev Cell* *14*, 205-215.
- Nunbhakdi-Craig, V., Machleidt, T., Ogris, E., Bellotto, D., White, C.L., 3rd, and Sontag, E. (2002). Protein phosphatase 2A associates with and regulates atypical PKC and the epithelial tight junction complex. *J Cell Biol* *158*, 967-978.
- Percival, A.C., and Slack, J.M. (1999). Analysis of pancreatic development using a cell lineage label. *Exp Cell Res* *247*, 123-132.
- Seymour, P.A., Freude, K.K., Tran, M.N., Mayes, E.E., Jensen, J., Kist, R., Scherer, G., and Sander, M. (2007). SOX9 is required for maintenance of the pancreatic progenitor cell pool. *Proc Natl Acad Sci U S A* *104*, 1865-1870.
- Soriano, P. (1999). Generalized lacZ expression with the ROSA26 Cre reporter strain. *Nat Genet* *21*, 70-71.
- Sorokin, L.M., Conzelmann, S., Ekblom, P., Battaglia, C., Aumailley, M., and Timpl, R. (1992). Monoclonal antibodies against laminin A chain fragment E3 and their effects on binding to cells and proteoglycan and on kidney development. *Exp Cell Res* *201*, 137-144.
- Tanentzapf, G., and Tepass, U. (2003). Interactions between the crumbs, lethal giant larvae and bazooka pathways in epithelial polarization. *Nat Cell Biol* *5*, 46-52.
- Wu, X., Li, S., Chrostek-Grashoff, A., Czuchra, A., Meyer, H., Yurchenco, P.D., and Brakebusch, C. (2007). Cdc42 is crucial for the establishment of epithelial polarity during early mammalian

development. *Dev Dyn* 236, 2767-2778.

Wu, X., Quondamatteo, F., Lefever, T., Czuchra, A., Meyer, H., Chrostek, A., Paus, R., Langbein, L., and Brakebusch, C. (2006). Cdc42 controls progenitor cell differentiation and beta-catenin turnover in skin. *Genes Dev* 20, 571-585.

Yu, W., Datta, A., Leroy, P., O'Brien, L.E., Mak, G., Jou, T.S., Matlin, K.S., Mostov, K.E., and Zegers, M.M. (2005). Beta1-integrin orients epithelial polarity via Rac1 and laminin. *Mol Biol Cell* 16, 433-445.

Zhou, Q., Law, A.C., Rajagopal, J., Anderson, W.J., Gray, P.A., and Melton, D.A. (2007). A multipotent progenitor domain guides pancreatic organogenesis. *Dev Cell* 13, 103-114.

## Figure and Figure legends

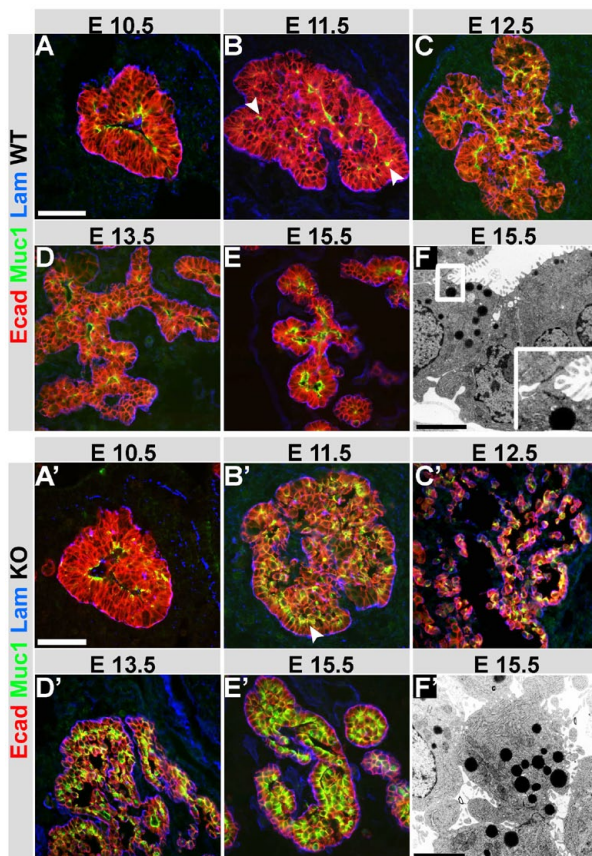


**Figure 1. Formation of tubes during pancreas development**

Representative sections of E10.5-15.5 pancreases (10  $\mu$ m) from WT and Cdc42 KO were stained with antibodies against mucin1 (Muc1; green), laminin (Lam; blue), and E-cadherin (Ecad; red), markers of the apical, basal and lateral domains, respectively.

(A-E) Within the WT multilayered epithelium microlumens were formed at E11.5 (indicated with arrowheads). Coordinated lumen expansion and tubulogenesis between E12.5-E15.5 resulted in the formation of fully polarized monolayered epithelium.

(A'-E') In Cdc42 KO epithelium no tubes were formed. Starting from E11.5, the apical marker, Muc1 was localized within cells (indicated with arrowhead), while Lam and Ecad distribution at the basolateral domains were normal. The lack of luminal network and aberrant epithelial morphology of the KO epithelium was evident from E12.5.

(F, F') TEM analysis of E15.5 WT pancreas shows a polarized epithelium with characteristic apical junctions (inset: magnification of the

indicated region) and microvilli. In contrast, Cdc42 KO pancreas shows failure to generate a fully polarized tubular morphology of the epithelium.

Scale bars, 50  $\mu$ m (A-E and A'-E'), 0.5  $\mu$ m (F and F').

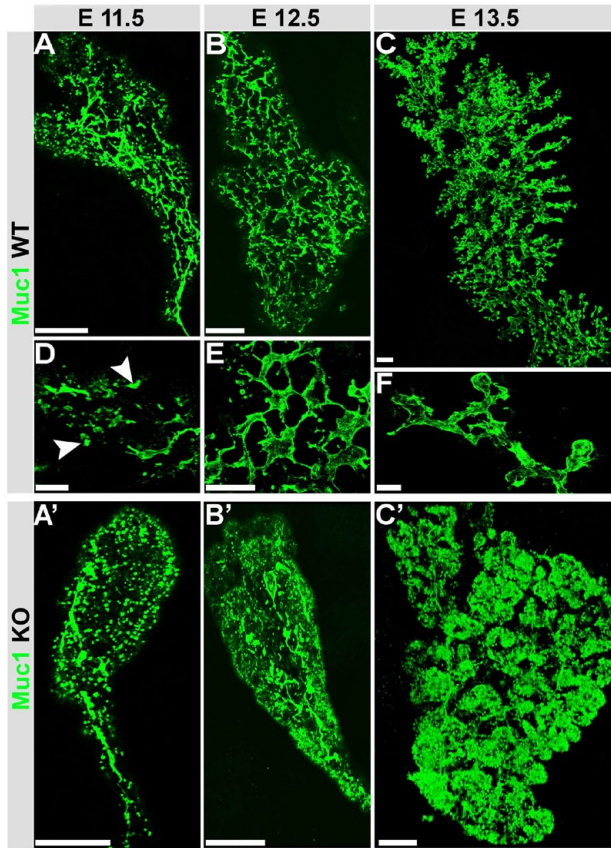


**Figure 2. Cdc42 is essential for tubulogenesis in the developing pancreas**

To characterize tubulogenesis in 3D, pancreases from E11.5- E13.5 were analyzed by whole-mount immunostaining with antibodies against mucin1 (Muc1; green), followed by 3D reconstructions of confocal images.

(A-C) In the WT, microlumens appeared stochastically at E11.5 (A). At 12.5 (B), microlumens expanded and coalesced into a continuous luminal network. At 13.5 (C), the initiated luminal network remodel into tubular structures.

(A'-C') In the Cdc42 KO aberrant luminal structures appeared at E11.5 (A'). The subsequent steps to generate a luminal network at E12.5 (B') and E13.5 (C') were blocked. The subcellular distribution of Muc1 was altered as well.

(D-F) To visualize tube formation in 3D at higher magnification, WT pancreas sections (40 $\mu$ m) were immunostained with antibodies against Muc1 (green). Microlumens

(indicated with arrowheads in D) were specifically observed at E11.5. Generation of a continuous luminal network (E12.5; E) and the first tubular structures (E13.5; F) define characteristic developmental stages during pancreatic tubulogenesis.

Scale bars, 50  $\mu$ m (A-C and A'-C'), 20  $\mu$ m (D-F).

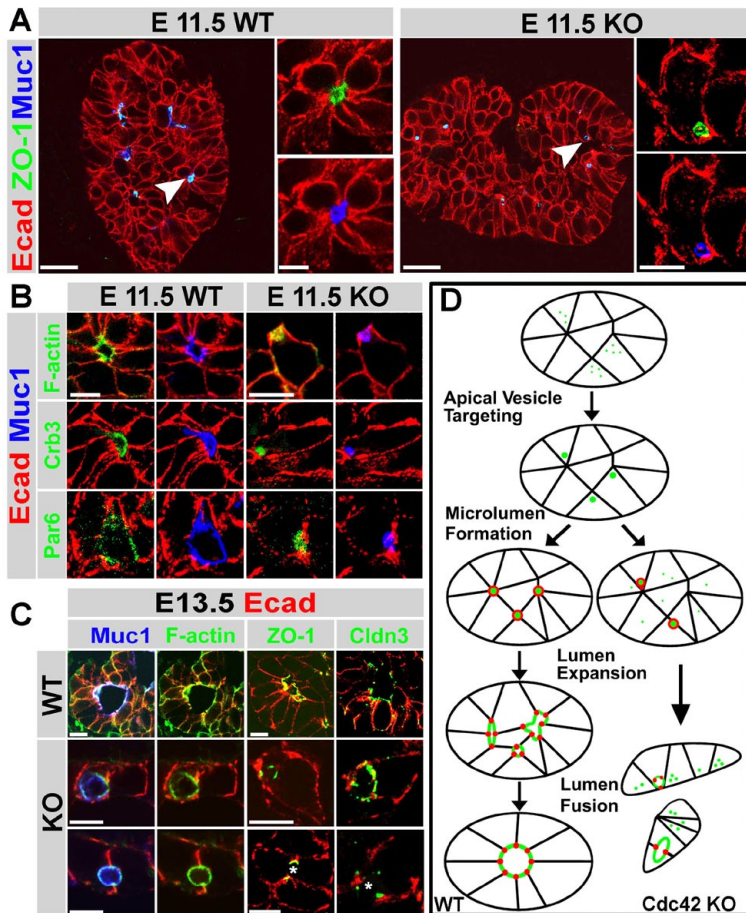


**Figure 3. Cdc42 is required for multicellular apical polarization**

E11.5 Pancreas sections were immunostained against the indicated antibodies and confocal images were acquired. (A) WT (left) and Cdc42 KO (right) pancreas sections were immunostained with antibodies against E-cadherin (Ecad; red), mucin1 (Muc1; blue), and ZO-1 (green). Within the WT epithelium multicellular lumens were formed. In contrast, auto-cellular lumens were observed within the Cdc42 KO epithelium. Magnified images of a WT microlumen (arrowhead; left) and a Cdc42 KO auto-cellular lumen (arrowhead; right) are shown in insets.

(B) WT (left) and Cdc42 KO (right) pancreas sections were immunostained with antibodies against Ecad (red), Muc1 (blue), and apical polarity markers: F-actin, crumbs3 (Crb3) and Par6 (green). The apical markers were distributed on the luminal surface of microlumen in the WT, whereas they were distributed on the luminal surface of auto-cellular lumens in the Cdc42 KO.

(C) E13.5 WT (left) and Cdc42 KO (right) pancreas sections were immunostained with antibodies against Ecad (red), Muc1 (blue), and tight junction (TJ) markers such as claudin3 (Cldn3), F-actin and ZO-1 (green). TJ proteins were normally distributed on the apical surface of the WT (top panel), whereas they were distributed on the auto-cellular lumens (middle panel) and intercellular lumen in the Cdc42 KO (bottom panel). Asterisks indicate intercellular lumen.

(D) Schematic illustration of microlumen formation. Cell polarization is triggered by the formation of vesicles carrying apical proteins (green). Targeting of vesicles and tight junctional complexes (red) establishes apical-basal cell polarity within single cells. Subsequently, neighboring cells undergo cell polarization resulting in the generation of microlumens with a common apical surface. Microlumen expansion and fusion establishes a luminal network. In contrast, the Cdc42 KO epithelium fails to generate a multicellular common apical surface, and instead forms auto-cellular and intercellular lumens. Scale bar, 20  $\mu$ m (A), 5  $\mu$ m (magnified panel; A) and 5  $\mu$ m (B,C)

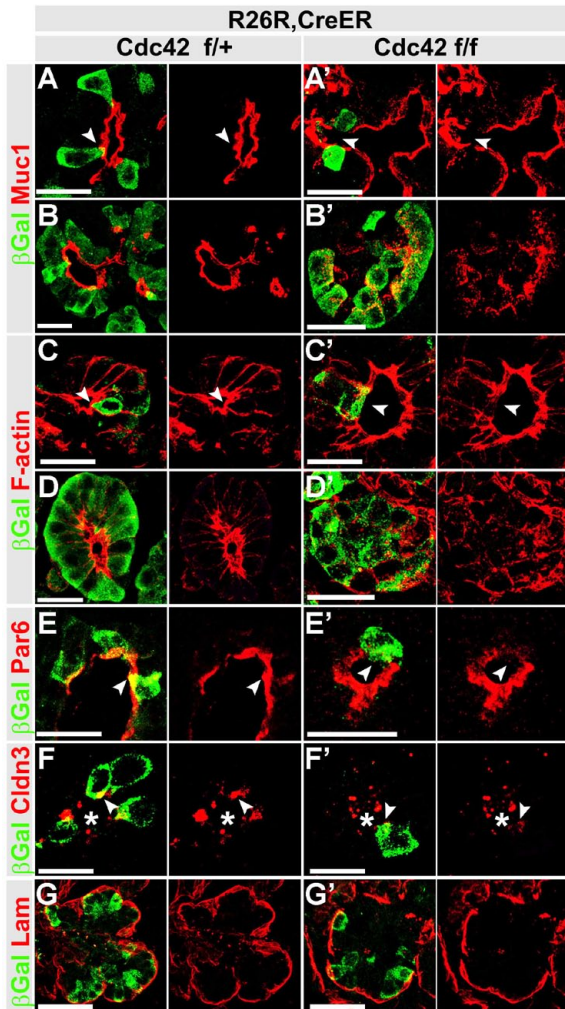


Figure 4. **Cdc42 is required for maintenance of tubes**

Cdc42 het (*Cdc42<sup>f/+</sup>; Pdx1-cre<sup>ER</sup>; R26R*) and Cdc42 KO embryos (*Cdc42<sup>f/f</sup>; Pdx1-cre<sup>ER</sup>; R26R*) were pulsed with TM at E12.5 and harvested at E15.5. The pancreas sections (10 μm) were immunostained with antibodies against beta-galactosidase (βGal; green) to mark the recombined cells and apical markers such as Muc1, F-actin, Par6 and Cldn3 (red). Arrowheads indicate individual βGal<sup>+</sup> cells distributed within the tubular epithelium. Asterisks indicate lumen (F).

(A-G) 3D reconstruction of confocal images showed polarized distribution of Muc1, F-actin, Par6 and Cldn3 on the apical surface of individual (indicated with arrowhead in A, C, E and F) and clustered βGal<sup>+</sup> cells (B and D). Laminin (Lam;red) was distributed on the basal surface.

(A'-G') Cdc42 KO pancreas lacked the polarized distribution of Muc1, F-actin, and Par6 (red) at the apical surface in both individual (indicated with arrowhead in A', C' and E') and clustered βGal<sup>+</sup> cells (B' and D'). Cldn3 was weak in the βGal<sup>+</sup> cells (F'). Distribution of laminin (Lam;red) on the basal surface remained unaffected (G').

Scale bar, 20 μm

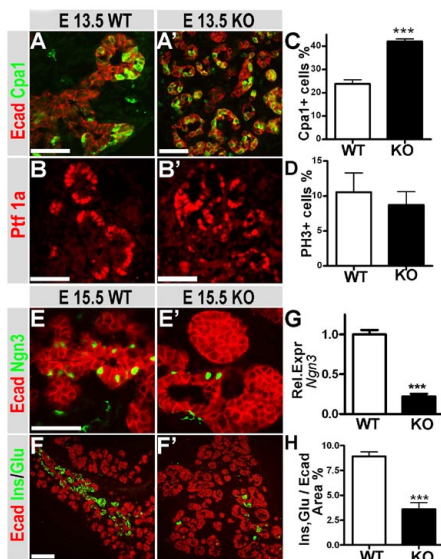


Figure 5. **Multipotent progenitors fail to differentiate towards endocrine lineages**

E13.5 WT and Cdc42 KO pancreas sections were immunostained with antibodies against E-cadherin (Ecad; red), carboxypeptidase A 1 (Cpa1; green), and Ptf1a (red).

(A, B) In the WT, Cpa1<sup>+</sup> and Ptf1a<sup>+</sup> cells were restricted to the tips.(A', B') In the Cdc42 KO, Cpa1<sup>+</sup> and Ptf1a<sup>+</sup> cells were randomly distributed and distinct tip and stalk morphology was absent.

(C) Proportion of Cpa1<sup>+</sup> cells versus the total number of epithelial cells (Ecad<sup>+</sup>) was increased in the KO pancreas. n=5, \*\*\*p<0.001.(D) Quantification of the mitotic index at E13.5 (phospho-histone H3; PH3<sup>+</sup>) versus the total number of epithelial cells (Ecad<sup>+</sup>) showed no change. n=3. (E, E') Fewer neurogenin3<sup>+</sup> (Ngn3<sup>+</sup>; green) cells were found in the E15.5 KO pancreas compared to WT. (F-F') Fewer and smaller clusters of insulin and glucagon (Ins/Glu; green) were observed in the E15.5 KO pancreas compared to WT.

(G) QPCR analysis from E14.5 KO pancreas showed a decrease in the relative expression (Rel.Expr) of *neurogenin3* (*Ngn3*). n=3, \*\*\*p<0.001 (H) Serial sections of E15.5 pancreas, stained for insulin, glucagon (Ins,Glu) and E-cadherin (Ecad). Ratio of Ins, Glu area to the total Ecad area was quantified (Axiovision). In the *Cdc42* KO, Ins<sup>+</sup>, Glu<sup>+</sup> cells were significantly reduced compared to WT. n=5, \*\*\*p<0.001. Error bars represent ± SEM. Scale bar, 50 μm.

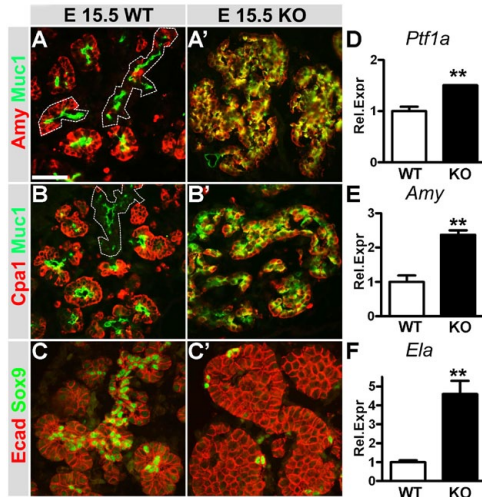


### Figure 6. *Cdc42* ablation results in increased acinar cell differentiation

E15.5 WT and *Cdc42* KO pancreas sections were immunostained with antibodies against amylase (Amy; red), carboxypeptidase A 1 (Cpa1; red), and mucin1 (Muc1; green). (A, B) In the WT, Amy<sup>+</sup> and Cpa1<sup>+</sup> cells were distributed at the branching tips. Muc1 staining indicates the luminal side of ducts (dotted lines). (A', B') In the *Cdc42* KO, Amy<sup>+</sup> and Cpa1<sup>+</sup> cells were found as epithelial aggregates. Ducts were absent. E15.5 pancreas sections were also immunostained with antibodies against E-cadherin (Ecad; red) and Sox9 (green). (C, C') In the WT, Sox9<sup>+</sup> cells were distributed along the stalk of the branching epithelium. Few Sox9<sup>+</sup> cells were scattered within the *Cdc42* KO epithelium. (D-F) QPCR mRNA expression analysis of E14.5 WT and *Cdc42* KO pancreases showed an increase in the relative expression of *Ptf1a* (D), *amylase* (*Amy*; E), and *elastase* (*Ela*; F). n=3, \*\*p<0.01. Error bars represent ± SEM. Scale bar, 50 μm.

(G) QPCR analysis from E14.5 KO pancreas showed a decrease in the relative expression (Rel.Expr) of *neurogenin3* (*Ngn3*). n=3, \*\*\*p<0.001 (H) Serial sections of E15.5 pancreas, stained for insulin, glucagon (Ins,Glu) and E-cadherin (Ecad). Ratio of Ins, Glu area to the total Ecad area was quantified (Axiovision). In the *Cdc42* KO, Ins<sup>+</sup>, Glu<sup>+</sup> cells were significantly reduced compared to WT. n=5, \*\*\*p<0.001. Error bars represent ± SEM. Scale bar, 50 μm.

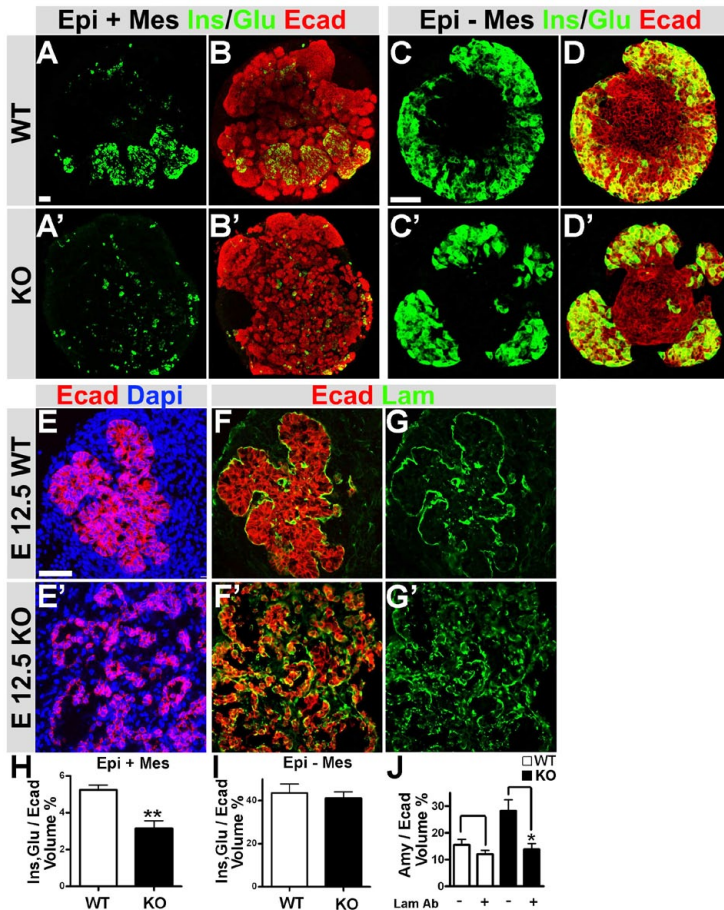


## Figure 7. **Cdc42 controls pancreatic cell fate decisions via cell-ECM interactions**

(A-D, A'-D') E11.5 WT and Cdc42 KO dorsal pancreases (DP) were cultured on filters for 7 days, fixed and whole-mount immunostained with antibodies against E-cadherin (Ecad; red), insulin and glucagon (Ins/Glu; green). Images represent 3D reconstructions of confocal images.

(A, B) In the WT DP (Epi + Mes), Ins<sup>+</sup>, Glu<sup>+</sup> cells were clustered in islet-like structures.

(A', B') In the Cdc42 KO DP (Epi + Mes), Ins<sup>+</sup> and Glu<sup>+</sup> cells were fewer and the distribution was scattered.

(C, D) WT epithelium without mesenchyme (Epi – Mes) preferentially differentiated into endocrine fates.

(C', D') Cdc42 KO epithelium (Epi – Mes) differentiated into endocrine cells with an efficiency that is comparable to WT epithelium.

(E-G, E'-G') E12.5 WT and Cdc42 KO pancreas sections were immunostained with antibodies against E-cadherin (Ecad; red) and Dapi (blue). Ecad<sup>-</sup> and Dapi<sup>+</sup> cells represent mesenchymal cells.

(E) In the WT, mesenchymal cells were distributed around the intact pancreatic epithelium.

(E') In the Cdc42 KO, the pancreatic epithelium was fragmented. Mesenchymal cells (Ecad<sup>-</sup>, Dapi<sup>+</sup>) were closely distributed between the epithelial fragments.

(F, G) Laminin (Lam; green) was distributed along the periphery of the branching epithelium.

(F', G') The epithelial fragments were in close contact with laminin (Lam; green) in the Cdc42 KO pancreas.

(H, I) The ratio of insulin and glucagon (Ins, Glu) volume to the total epithelial volume (Ecad volume) was calculated. (H) In the Cdc42 KO (Epi + Mes), endocrine cell differentiation was reduced. n=4, \*\*p<0.01. (I) In contrast, both WT and Cdc42 KO (Epi – Mes) showed no difference in endocrine differentiation, n=5.

(J) E11.5 WT and Cdc42 KO explants were treated with a laminin-1 functional-blocking antibody (Lam Ab + added on day 1, 3 and 5) and compared with untreated controls (Lam Ab -). By morphometric analysis the ratio of amylase to Ecad volume was calculated. Notably, acinar cell differentiation in the Cdc42 KO was restored to WT levels when laminin-1 was functionally blocked. n=4, \*p<0.05.

Error bars represent ± SEM. Scale bars, 20 μm (A-D and A'-D'), 50 μm (E-G and E'-G')

# Supplemental Data

## **Cdc42-mediated tubulogenesis controls cell specification**

Gokul Kesavan<sup>1</sup>, Fredrik Wolfhagen Sand<sup>1</sup>, Thomas Uwe Greiner<sup>1</sup>, Jenny Kristina Johansson<sup>1</sup>, Sune Kobberup<sup>1</sup>, Xunwei Wu<sup>2</sup>, Cord Brakebusch<sup>2</sup>, Henrik Semb<sup>1</sup>

## **Supplementary Experimental procedures**

### **In situ hybridization**

The complete cDNA of *Cdc42* ( Imagene) was linearised, labeled with digoxigenin using T3 and T7 RNA polymerase (Roche) to generate sense and antisense probes according to standard procedure. 1 µg/ml of the probes were hybridized overnight on cryosections (8µm) and processed as previously described (Corbetta et al., 2005)

### **Quantitative PCR**

The PCR conditions were followed as previously described and the primer sequences are presented in supplementary table 2 (Gao et al., 2007; Masui et al., 2007).

### **Immunoblotting**

Embryonic pancreases and dorsal pancreatic explants were lysed in lysis buffer (10 mM Tris HCL, 66 mM EDTA, 150 mM NaCl, 0.4% NaDeoxycholate and 1% NP- 40) for one hour. The samples were boiled for five minutes in Sample Buffer (100 mM TRIS, 4% (w/v) SDS, 0.2% (w/v) bromophenol blue, 20% (w/v) glycerol, 200 mM β-mercaptoethanol), centrifuged for five minutes at 5900 G. Samples were separated on SDS-PAGE and transferred onto a nitrocellulose membrane (Amersham). The membrane was blocked for one hour in PBS-0.1% Tween-20 containing 5% dry milk or 3% BSA and blotted with primary antibodies against aPKC (1:500; Santa Cruz), alpha Tubulin (1:1000; Sigma) and Cdc42 (1:200; BD Bioscience) overnight at 4°C in blocking solution. The blot was incubated with HRP-conjugated secondary antibodies for one hour and proteins were visualized by chemiluminescence (Amersham).

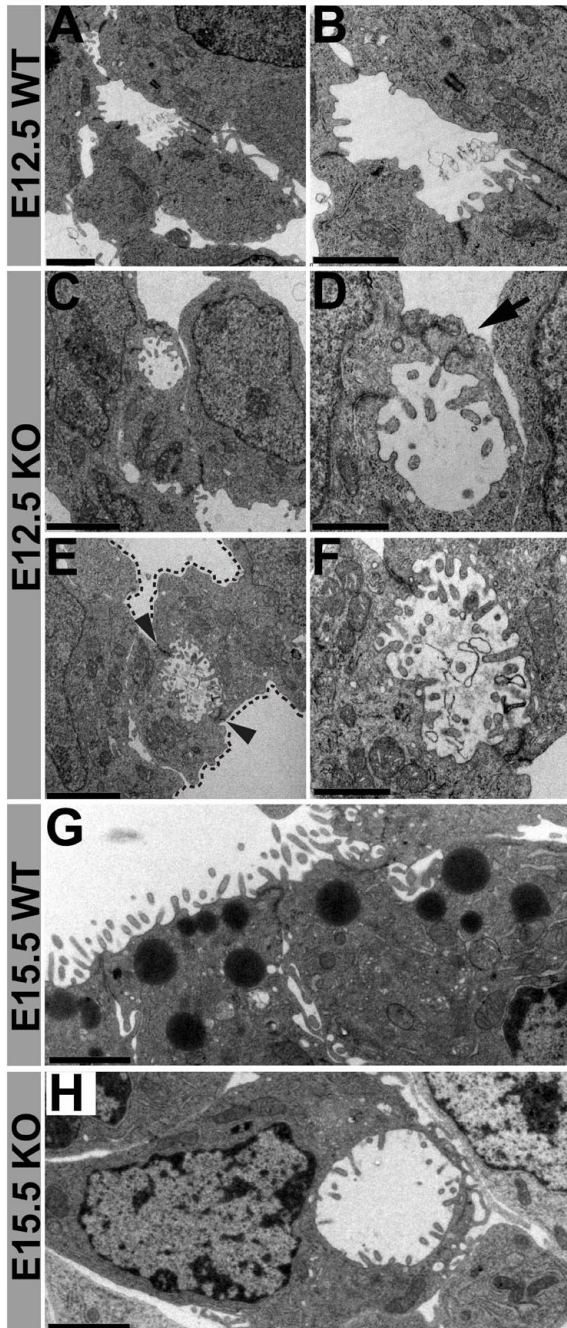


**Figure S1. Ultrastructural details of microlumens**

(A, B) TEM images of E12.5 WT pancreas showing the apical surface shared between several neighboring cells. Microvilli and apical junctions are observed on the luminal surface.

(C, D) TEM images of E12.5 Cdc42 KO pancreas showing an autocellular lumen. Notably, the autocellular lumen is covered by microvilli and is in direct contact with cell surface through autacellular junctions (indicated with arrow).

(E, F) TEM images of E12.5 Cdc42 KO pancreas showing an intercellular lumen between two neighboring cells (cell surfaces are indicated with dots). Apical junctions at cell-cell contacts are indicated with arrowheads.

(G) TEM analysis of E15.5 WT pancreas showing microvilli and mature cell-cell junctions on the luminal surface.

(H) TEM analysis of E15.5 Cdc42 KO pancreas showing a large autocellular lumen covered with microvilli-like structures.

Scale bars, 1  $\mu\text{m}$  (A, C, E, G and H), 0.5  $\mu\text{m}$  (B, D and F).

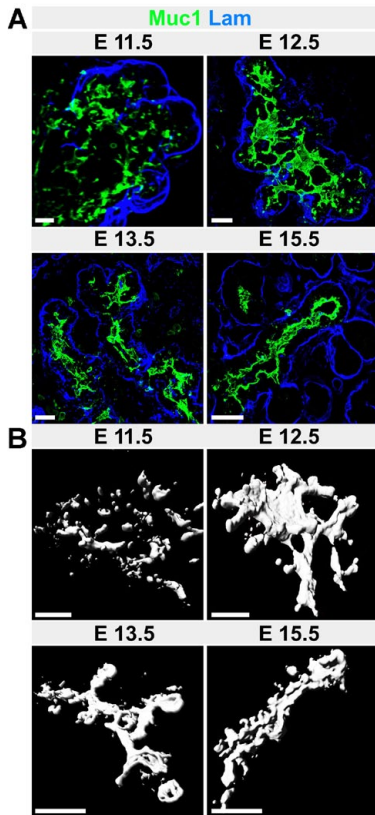


**Figure S2. 3D architecture of epithelial-ECM interactions during pancreatic tubulogenesis**

To characterize tubulogenesis and cell polarity in 3D, WT pancreas sections (40  $\mu\text{m}$ ) from E11.5- E15.5 were analyzed by immunostaining with antibodies against mucin1 (Muc1; green) and laminin (Lam; blue), followed by 3D reconstructions of confocal images.

(A) At E11.5, laminin (Lam; blue) was restricted to the periphery of the multilayered pancreatic epithelium. As cell polarization and tubulogenesis progressed, laminin covered the entire tubular monolayered epithelium.

(B) To visualize the key steps in tubulogenesis, isosurface renderings (Imaris) on the Muc1 immunostainings from representative regions of E11.5 to E15.5 WT pancreases were carried out. The images were oriented to visualize the 3D architecture of each characteristic stage in tube formation.

Scale bars, 20  $\mu\text{m}$

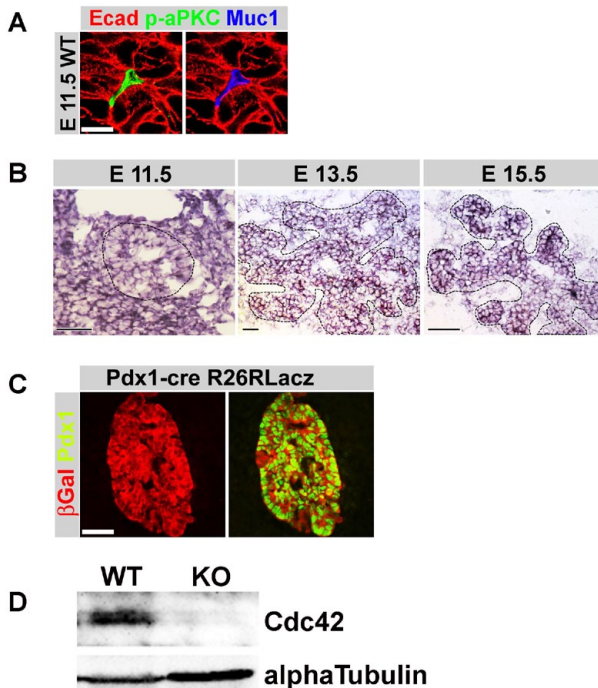


**Figure S3. Cdc42 and p-aPKC expression in the developing pancreas, and Pdx1 cre-recombination efficiency**

(A) E11.5 WT pancreas sections were immunostained with antibodies against E-cadherin (Ecad; red), mucin1 (Muc1; blue), and phosphorylated aPKC (p-aPKC; green). p-aPKC co-localized with Muc1 on the apical surface of microlumens.

(B) In situ hybridization analysis of *Cdc42* mRNA showing ubiquitous expression in the pancreatic epithelium (indicated with dotted lines). At earlier stages *Cdc42* mRNA is also expressed in the mesenchyme.

(C) To evaluate recombination efficiency at E11.5, *Pdx1-cre* mice were crossed with *R26RLacZ* reporter mice. The beta-galactosidase ( $\beta\text{Gal}$ ; red) staining overlapped completely

with Pdx1 (green), and demonstrated efficient recombination at this stage (90-95%).

(D) Western blot analysis on E17.5 WT and Cdc42 KO pancreases demonstrated efficient deletion of Cdc42 in the KO. Alpha Tubulin was included in the analysis as a reference protein. Scale bars, 10  $\mu\text{m}$  (A) and 50  $\mu\text{m}$  (B, C)

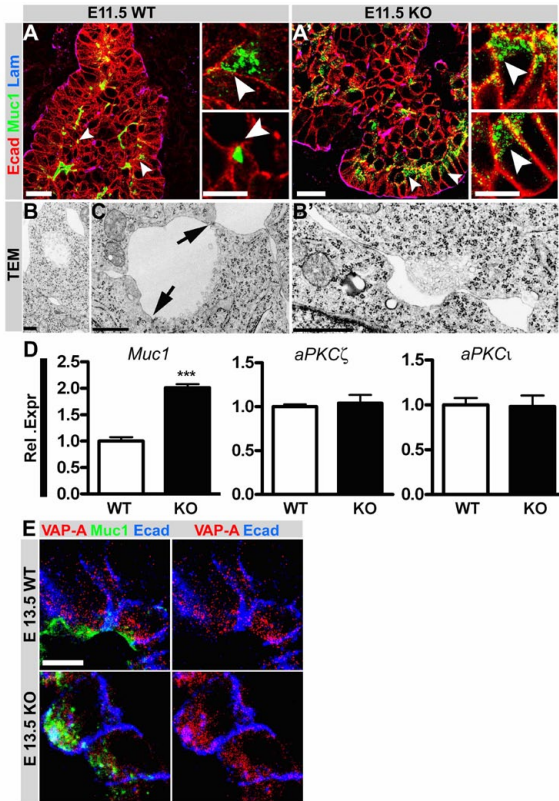


#### Figure S4. Apical cell polarization in single cells

(A) E11.5 WT pancreas sections were immunostained with antibodies against E-cadherin (Ecad; red), mucin1 (Muc1; green), and laminin (Lam; blue). Polarized targeting of Muc1-containing vesicle aggregates were observed within single cells. The regions indicated with arrowhead are magnified in the adjacent panels.

(A') In the E11.5 Cdc42 KO pancreas vesicular aggregates of Muc1 were observed. More Muc1<sup>+</sup> cells were observed in the Cdc42 KO pancreas compared to the WT. The regions indicated with arrowhead are magnified in the adjacent panels.

(B) TEM analysis of E11.5 WT pancreas showing polarized distribution of vesicle aggregates.

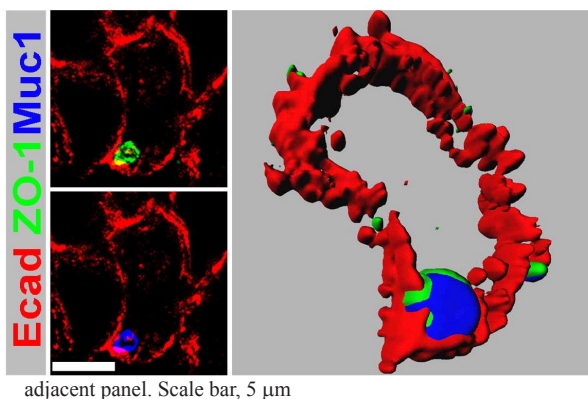
(C) Targeting of vesicles to the de novo apical surface of E11.5 WT pancreas. Notably, this is only observed in individual cells. Concomitantly, primitive cell-cell junctions on the apical surface are observed (indicated with arrows).

(B') TEM analysis of E11.5 Cdc42 KO pancreas showing vesicle aggregates at the cell surface.

(D) Q-PCR mRNA expression analysis of E14.5 WT and Cdc42 KO pancreases showing an increase in the relative expression of *Muc1* in the Cdc42 KO. In contrast, neither *aPKC $\zeta$*  nor *aPKC $\iota$*  mRNA expression changed upon Cdc42 ablation. n=5 (WT) and n=3 (KO), \*\*\*p<0.001.

(E) E13.5 WT and KO pancreas sections were immunostained with antibodies against VAMP associated protein A (Lapierre et al., 1999) (VAP-A; red), mucin1 (Muc1; green) and E-cadherin (Ecad; blue). No morphological differences were observed on the sub-apical distribution of VAP-A marked vesicles between the WT and Cdc42 KO pancreases.

Error bars represent  $\pm$  SEM. Scale bars, 20  $\mu\text{m}$  (A and A'), 5  $\mu\text{m}$  (magnified panels) and 1  $\mu\text{m}$  (B, C and B')



adjacent panel. Scale bar, 5  $\mu\text{m}$

#### Figure S5. 3D reconstruction of an autocellular lumen

To visualize autocellular lumens three dimensionally in the Cdc42 KO, we generated isosurface renderings and 3D reconstruction images of E-cadherin (Ecad; red), ZO-1 (green) and Muc1 (blue) immunostainings shown in figure 3A. The 3D reconstruction was carried out on 10  $\mu\text{m}$  thick pancreas section. For convenience we present the original figure (extracted from Figure 3A) in the

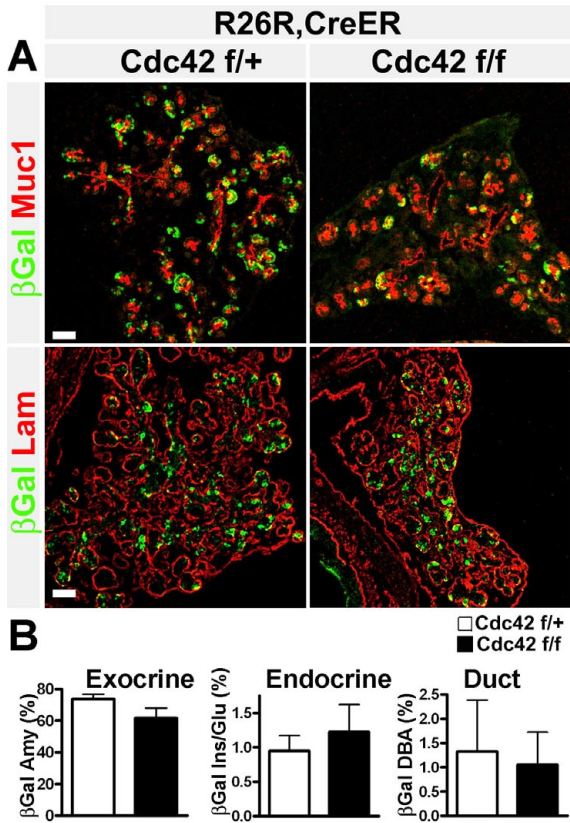


**Figure S6. Mosaic deletion of Cdc42 does not affect cell fate specification**

(A) Cdc42 het and KO embryos (*Cdc42*<sup>f/+</sup>; *Pdx1-cre*<sup>ER</sup>; *R26R* and *Cdc42*<sup>f/f</sup>; *Pdx1-cre*<sup>ER</sup>; *R26R*) pulsed with TM at E12.5 and harvested at E15.5 were immunostained with antibodies against beta-galactosidase (βGal; green), mucin1 (Muc1; red) and laminin (Lam; red). Muc1 and laminin immunostainings demonstrated that mosaic deletion of Cdc42 does not affect the overall tissue architecture, i.e. the tubular network is intact.

(B) Serial sections of E15.5 pancreas from Cdc42 het and KO embryos were immunostained with antibodies against beta-galactosidase combined with exocrine marker amylase or endocrine marker insulin and glucagon or duct marker DBA. Percentages of βGal<sup>+</sup> cells co-expressing either of the three lineage specific markers were quantified. Graphs represent the percentage of βGal cells co-expressing each one of the indicated markers. No significant differences in any of the three lineage specification were observed. n=4, p>0.05.

Error bars represent ± SEM. Scale bars, 20 μm.

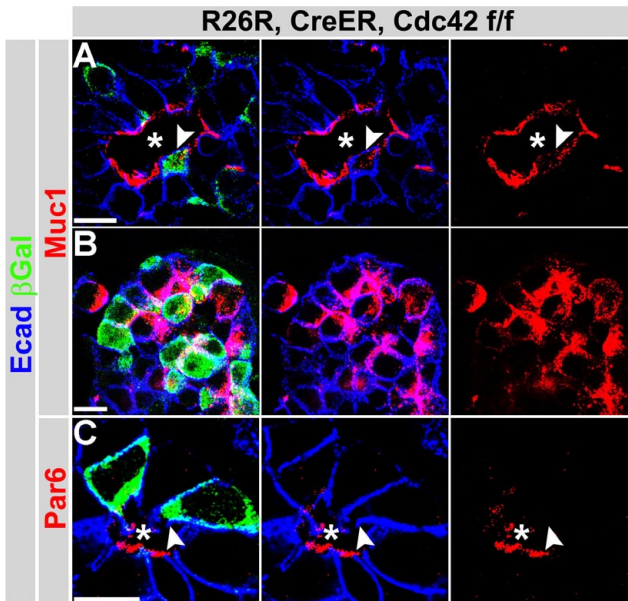


**Figure S7. Cdc42 is required for maintenance of apical polarity**

*Cdc42*<sup>f/f</sup>; *Pdx1-cre*<sup>ER</sup>; *R26R* embryos were pulsed with TM at E12.5 and harvested at E15.5. Pancreas sections (10 μm) were immunostained with antibodies against E-cadherin (Ecad; blue) marking the epithelium, beta-galactosidase (βGal; green) to mark the recombined cells, and apical markers, including mucin1 (Muc1) and Par6 (red). Confocal images are shown.

Cdc42 ablation resulted in loss of polarized distribution of Muc1 (A, B) and Par6 (C) at the apical surface in βGal<sup>+</sup> individual intra-ductule epithelial cells (arrowheads in

A and C) as well as in clustered extra-ductule βGal<sup>+</sup> cells (B). The loss of apical membrane in the Cdc42 KO cells was compensated with lateral membrane, marked by E-cadherin. Asterisk indicates lumen (A and C). Scale bar, 10 μm

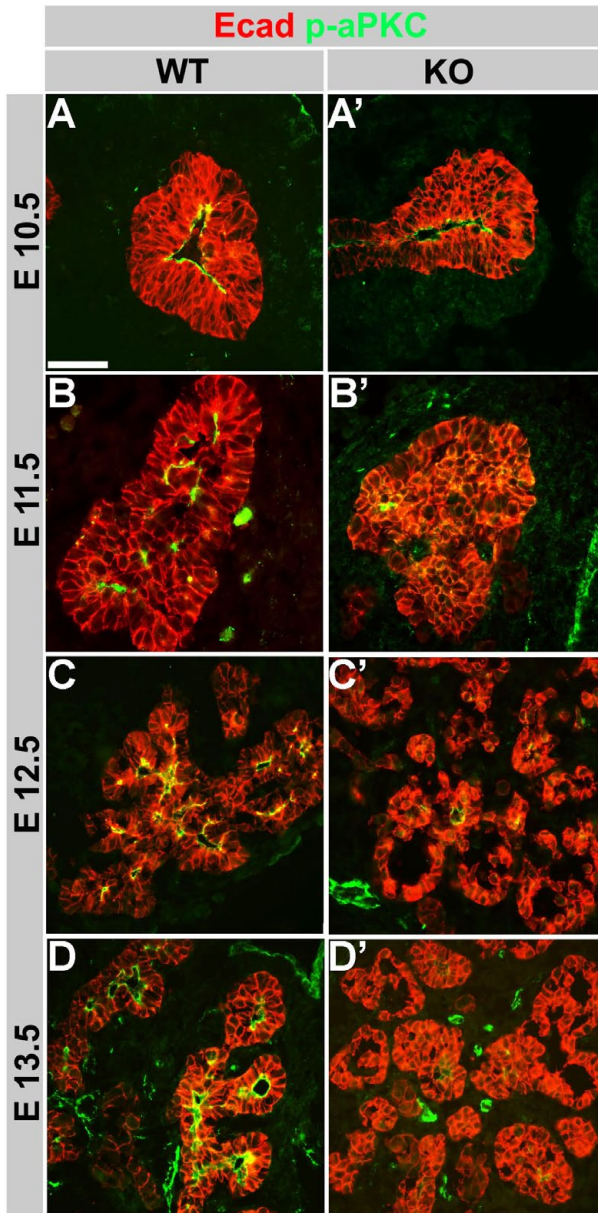


**Figure S8. aPKC activity is undetectable in Cdc42 KO epithelium**

Pancreas sections from E10.5-15.5 were immunostained with antibodies against E-cadherin (Ecad; red) and phosphorylated aPKC (p-aPKC; green).

(A-D) In the WT pancreas, apical localization of p-aPKC (green) was observed in the WT branching epithelium from E10.5 to E 13.5. p-aPKC was also expressed in the blood vessels.

(A'-D') In the Cdc42 KO pancreas, most of the p-aPKC expression within the epithelium was lost between E10.5 and E11.5. At E13.5, it was no longer detectable within the epithelium. Notably, blood vessel p-aPKC was unaffected in the Cdc42 KO pancreas (*Pdx1-cre* is epithelial-specific).

Scale bars, 50  $\mu$ m.

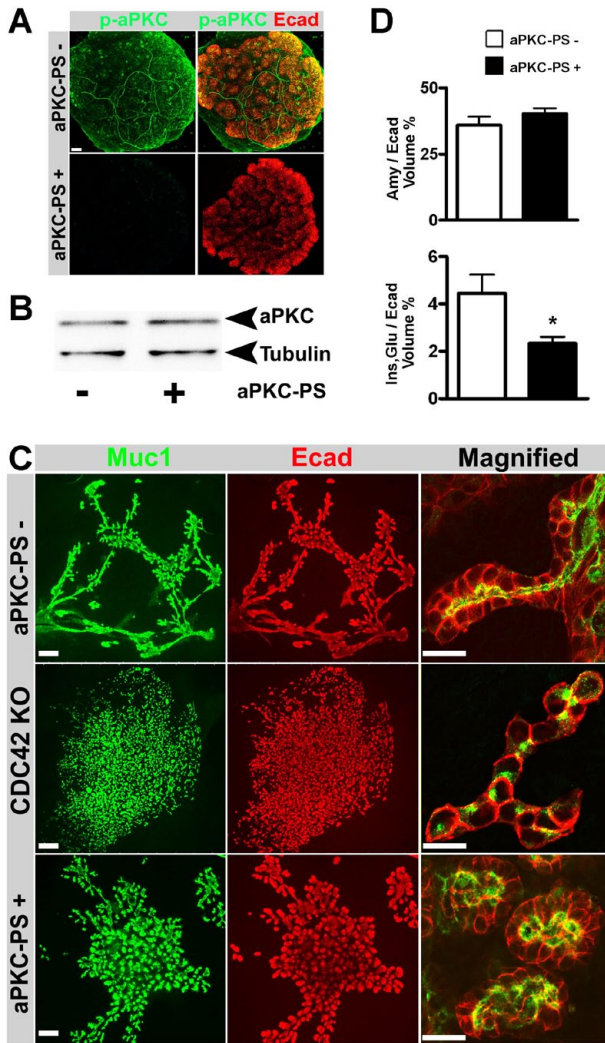


**Figure S9. aPKC-PS blocks activation of aPKC leading to a discontinuous tubular network**

(A) E11.5 WT dorsal pancreas was cultured as explants and treated with a myristoylated substrate of aPKC- $\zeta$  (aPKC-PS; 40  $\mu\text{g}/\text{ml}$ ). The explants were fixed after 1 day of aPKC-PS treatment and immunostained with antibodies against phosphorylated aPKC (p-aPKC; green) and E-cadherin (Ecad; red). p-aPKC is strongly expressed both in the mesenchyme including the blood vessels and in the epithelium.

(B) Protein lysates from the aPKC-PS treated and untreated explants were analyzed by western blotting showed no change in the expression levels of endogenous aPKC between the samples. Alpha Tubulin was included in the analysis as a reference protein.

(C) E11.5 dorsal pancreas cultured as 2D explants were immunostained with antibodies against Muc1 (green) and E-cadherin (Ecad; red). Confocal microscopy was used to generate high magnification images (Magnified). WT explants developed a highly

branched tubular network. In contrast, Cdc42 KO explants failed to form tubes and Muc1 was distributed intracellularly. WT explants treated with aPKC-PS (40  $\mu\text{g}/\text{ml}$  on day 1, 3 and 5) failed to establish a tubular network, but Muc1 distribution was unaffected. Images show representative pictures of 4 independent experiments with 3-4 samples in each group.

(D) WT explants treated with aPKC-PS (aPKC-PS+) and the untreated controls (aPKC-PS-) were fixed on day 7 and immunostained with antibodies against E-cadherin (Ecad), amylase (Amy), insulin and glucagon (Ins,Glu). Morphometric analysis was carried out on the 3D reconstructed images and the ratio of both Ins/Glu volume to the total epithelial volume (Ecad volume) and Amy to total volume was calculated using Imaris software. Explants treated with aPKC-PS showed a decrease in endocrine differentiation, whereas the acinar differentiation remained unaffected.  $n=4$  \* $p < 0.05$ . Error bars represent  $\pm$  SEM. Scale bars, 50  $\mu\text{m}$  (A), 50  $\mu\text{m}$  (C) and 20  $\mu\text{m}$  (C; Magnified).

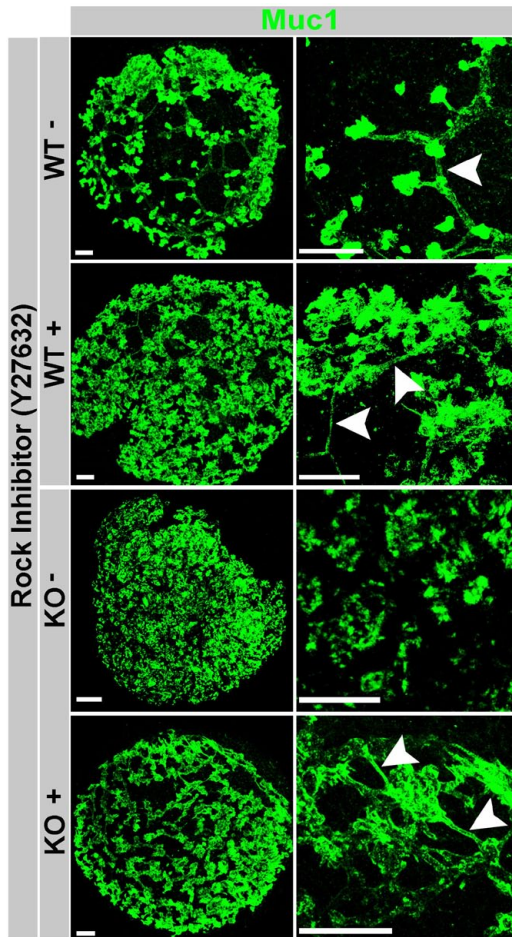


**Figure S10. Blocking ROCK activity restores tube formation in Cdc42 KO epithelium**

E11.5 WT and Cdc42 KO dorsal pancreases (DP) were harvested (day 0) and cultured on filters. The explants were treated with the pharmacological inhibitor of ROCK I/II (Y27632, 10  $\mu$ M) from day 1 onwards (WT + and KO +) and were compared with untreated controls (WT - and KO -). The explants were fixed on day 6, immunostained with antibody against Mucin 1 (Muc1; green) and 3D reconstructions of confocal images were generated. Images show representative pictures of 3 independent experiments. WT explants developed a highly branched tubular network. Treatment of WT pancreatic explants with Y27632 did not affect tube formation. Cdc42 KO explants failed to form tubes however treating them with Y27632 rescued tube formation. Arrowheads indicate tubes.

Scale bars, 50  $\mu$ m

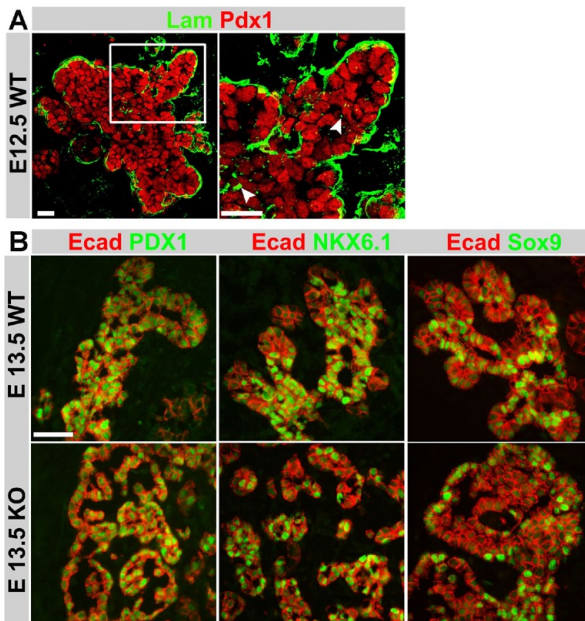


**Figure S11. Multipotent pancreatic progenitors express characteristic lineage determining transcription factors**

(A) Thick sections (40  $\mu$ m) of WT pancreases were immunostained with antibodies against Pdx1 (red) and laminin (Lam; green). 3D reconstructed confocal images show continuous organization of laminin around the peripheral cells. Few spots of laminin could be observed within the core of the multilayered epithelium (indicated with arrowheads). However, laminin assembly does not overlap with the forming microlumens. The white box indicates the region magnified in the adjacent panel.

(B) E13.5 pancreas sections were immunostained with antibodies against E-cadherin (Ecad; red) and

multipotent progenitor markers of the pancreas such as Pdx1, Nkx 6.1, and Sox9 (green). No difference in the expression pattern of these transcription factors in the WT and Cdc42 KO pancreas was observed. Scale bars, 20  $\mu\text{m}$  (A) and 50  $\mu\text{m}$  (B).

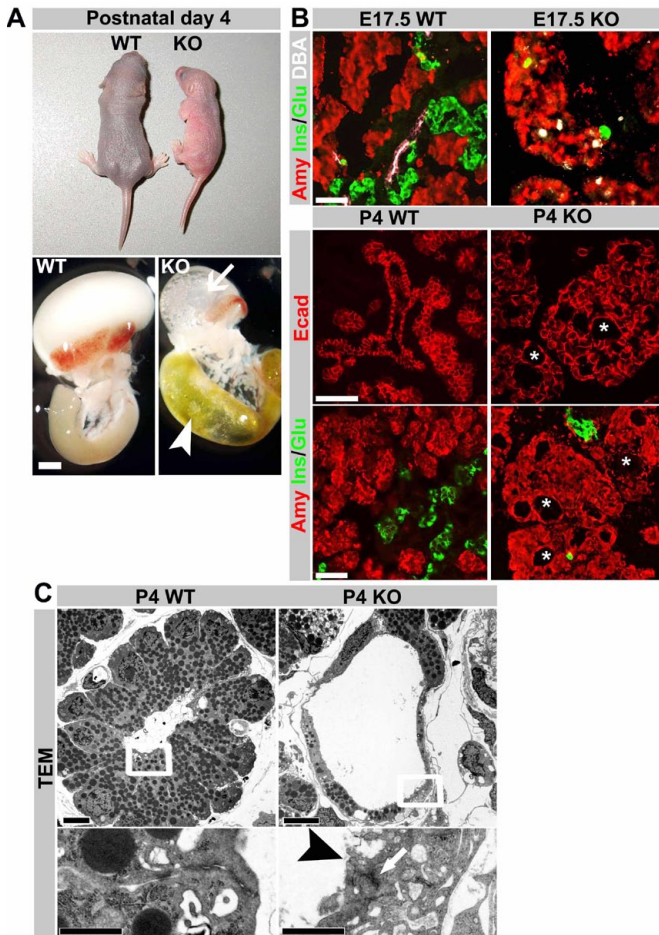


### Figure S12. Cdc42-deficient animals develop postnatal pancreatic and duodenal phenotypes

(A) The Cdc42 KO pups were growth retarded and developed distended duodenum (indicated with arrowhead) and cystic stomach (indicated with arrow). The KO pups were terminated around postnatal day 4 (P4) for ethical reasons.

(B) Pancreas sections from E17.5 and Postnatal day 4 (P4) were immunostained with antibodies against amylase (Amy; red), insulin and glucagon (Ins/Glu; green), dolichos biflorus agglutinin (DBA; white) and E-cadherin (Ecad; red). At E17.5, very few endocrine and duct cells were randomly distributed between acinar clusters within the Cdc42 KO pancreas. At P4, cystic acinar clusters developed in the Cdc42 KO pancreas (indicated with asterisk).

(C) TEM analysis of P4 WT

pancreas showed characteristic acini with well organized lumens, whereas cysts formation was apparent within the Cdc42 KO acinar clusters. Organization of actin bundles representing tight junctions were found on the apical surface of the cysts in Cdc42 KO pancreas (arrow and arrowhead indicate the actin bundles and their opening to the apical surface, respectively). Insets indicated with white squares are magnified in the bottom panel.

Scale bars, 1000  $\mu\text{m}$  (A), 50  $\mu\text{m}$  (B), 5  $\mu\text{m}$  (C) and 1  $\mu\text{m}$  (magnified inset).

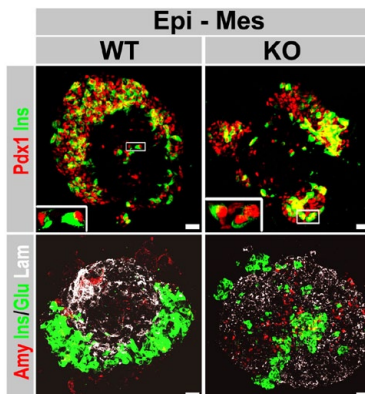


### Figure S13. Characterization of endocrine and exocrine lineages in mesenchyme-depleted pancreatic explants

E11.5 WT and Cdc42 KO dorsal pancreatic explants depleted of mesenchyme (Epi - Mes) were cultured on filters for 7 days, fixed and immunostained with antibodies against Pdx1 (red), insulin and glucagon (Ins/Glu; green), amylase (Amy; red) and laminin (Lam; white). Images represent 3D reconstructions of confocal images.

Ins<sup>+</sup> cells within WT and Cdc42 KO explants expressed high levels of Pdx1 (inset; magnification of the indicated region). High Pdx1 in Ins<sup>+</sup> cells indicates that these beta cells represent secondary transition insulin<sup>+</sup> cells. Acinar differentiation in mesenchyme-depleted explants was severely compromised.

Very few Amy<sup>+</sup> cells and weak laminin distribution was observed both in WT and KO explants.  
Scale bar, 20  $\mu$ m

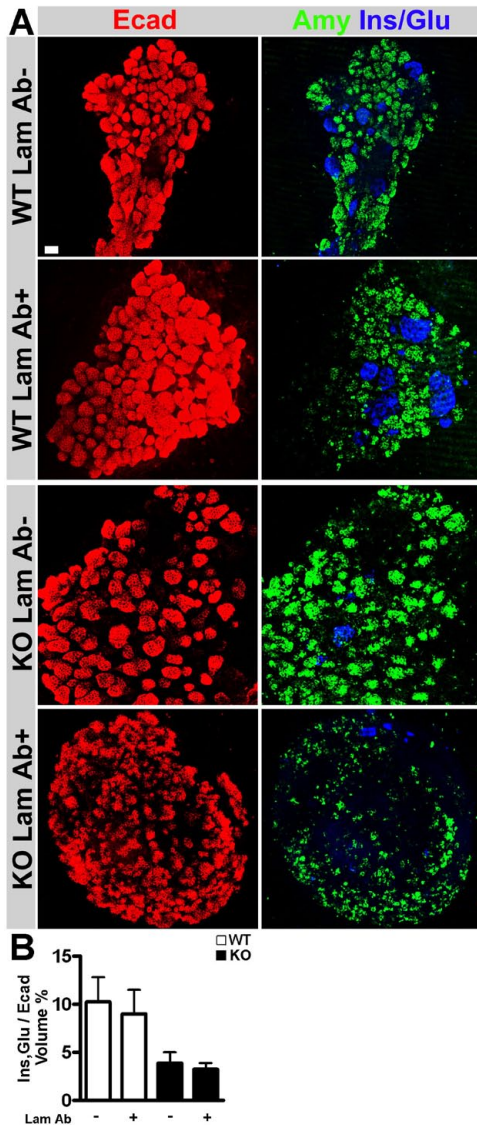


**Figure S14. Inhibition of laminin-1 in Cdc42 KO explants restores acinar differentiation to WT levels**

E11.5 WT and Cdc42 KO dorsal pancreases (DP) were cultured as 2D explants. They were treated with a laminin-1 functional-blocking antibody (Lam Ab + added on day 1, 3 and 5) E11.5 WT and Cdc42 KO and were compared with untreated controls (Lam Ab -). The explants were fixed and whole-mount immunostained with antibodies against E-cadherin (Ecad; red), insulin and glucagon (Ins/Glu; blue) and amylase (Amy; green). Images represent 3D reconstructions of confocal images.

(A) Comparing untreated (WT Lam Ab-) and treated WT explants (WT Lam Ab+) showed a trend towards reduced acinar differentiation in the presence of the laminin antibody. Importantly, the antibody reduced the enhanced acinar commitment in the Cdc42 KO (KO Lam Ab+) to WT levels (quantified in Fig. 7).

(B) From the 3D reconstructed images, the ratio of Ins/Glu to Ecad volume was calculated (morphometric analysis using Imaris). Inhibition of laminin-1 in Cdc42 KO explants failed to rescue endocrine differentiation, whereas acinar differentiation was restored (see Figure 7J). n=4

Error bars represent  $\pm$  SEM. Scale bar, 50  $\mu$ m

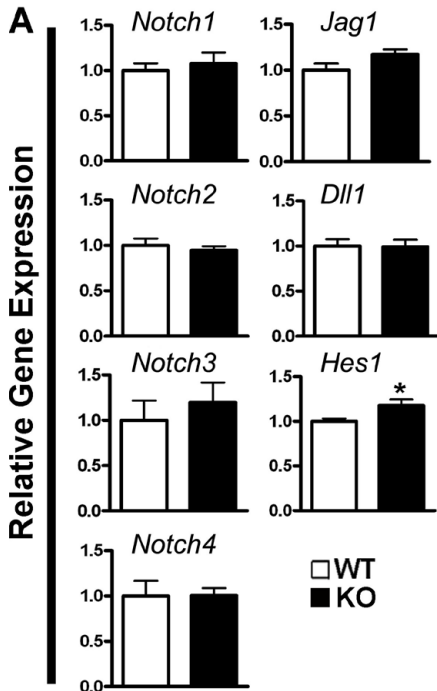


**Figure S15. mRNA expression of notch receptors, ligands and targets**

(A) Q-PCR mRNA expression analysis of Notch receptors, ligands and targets in E14.5 WT and Cdc42 KO pancreases. Except for *Hes1*, which was slightly upregulated in the Cdc42 KO, no change in the expression of Notch receptors and ligands was observed. n=5 (WT) and n=3 (KO), \*p<0.05

(B) E11.5 WT and Cdc42 KO dorsal pancreases (DP) were cultured as 2D explants and treated with the gamma secretase inhibitor (10  $\mu$ M DAPT in 0.1% DMSO; Sigma) on day 2. The day of harvest d=0. The controls were treated with DMSO (0.1%). The explants were fixed on day 5 and immunostained with antibodies against E-cadherin (Ecad), insulin (Ins) and glucagon (Glu). Morphometric analysis of 3D reconstructed images was used to quantify the ratio of the Ins/Glu volume to the total epithelial volume (Ecad volume). DAPT treatment stimulated endocrine differentiation in WT explants, whereas it failed to affect endocrine differentiation in Cdc42 KO explants. n=4 (WT) and n=3 (KO) \* p< 0.05 Error bars represent  $\pm$  SEM.

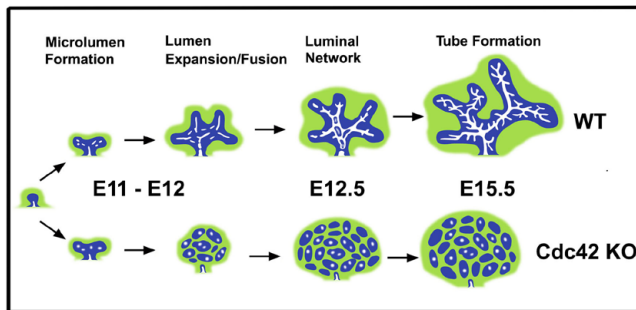
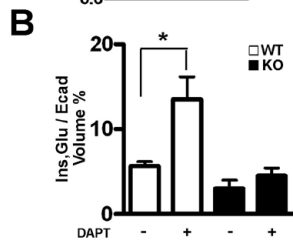


**Figure S16. Model of tube formation in the developing pancreas.**

Schematic figure of tubulogenesis in the WT and Cdc42 KO pancreas.

In the WT, tubulogenesis is initiated at E11.5 by formation of microlumens (white) within the multilayered unpolarized pancreatic epithelia (blue), which is surrounded by mesenchyme (green). Between E11.5-12.5, the microlumens expand and coalesce to generate a continuous luminal network. Subsequently, this luminal network remodels to form tubes between E13.5- E15.5. Cdc42 is required for microlumen formation. The failure to initiate tubulogenesis in Cdc42 KO animals results in aberrant epithelial cell-ECM interactions, which cause aberrant cell fate specification.

**Supplementary table 1. List of antibodies used**

Antibody	Raised in	Dilution	Source
Amylase	Goat	1:1000	Sigma
Amylase	Rabbit	1:500	Sigma
aPKC	Rabbit	1:100	Santa cruz
Beta Galactosidase	Rabbit	1:1000	ICN
Beta Galactosidase	Chicken	1:250	Abcam
Cdc42	Mouse	1:200	BD bioscience
Claudin3	Rabbit	1:100	Invitrogen
Cleaved Caspase-3	Rabbit	1:1000	R&D systems
Cpa1	Rabbit	1:500	Biogenesis
Crumbs3	Rabbit	1:200	B.Margolis
DBA		1:1000	Vector
Ecadherin	Rat	1:200	Takara
F-actin		1:500	Invitrogen
Glucagon	Guinea pig	1:800	Linco
Insulin	Guinea pig	1:800	Linco
Laminin-1	Rat	200µg/ml	M.Durbeej
Mucin 1	Armenian hamster	1:500	Neomarkers
Neurogenin3	Mouse	1:2000	BCBC
Nkx6.1	Rabbit	1:2000	BCBC
Pan-laminin	Rabbit	1:500	Sigma
Par6B	Rabbit	1:100	S.Ohno
Pdx1	Guinea pig	1:500	C.Wright
Phospho-aPKC	Rabbit	1:50	Cell signaling
Ptf1a	Rabbit	1:1000	BCBC
Sox9	Rabbit	1:800	Chemicon
VAP-A	Rabbit	1:100	Sigma
ZO-1	Rabbit	1:100	Invitrogen

**Supplementary table 2. QPCR primers**

Gene	Primer Pair
Amylase2	5'-AGGTCATTGATCTGGGTGGTG-3' 5'-GACATCTTCTCGCCATTCCAC-3'
Elastase1	5'-AGCAGA ACCTGAGCCAGAAT-3' 5'-TTGTTAGCCAGGATGGT TCC-3'
HPRT	5'-AGCCCCAAAATGGTTAAGGT-3' 5'-CAAGGGCATATCCAACAACA-3'
Ngn3	5'-TGGCCCATAGATGATGTTTCG-3' 5'-AGAAGGCAGATCACCTTCGTG
Ptf1a	5'-CTTGCAGGGCACT CTCTTTC-3' 5'-CGATGTGAGCTGTCTCAGGA-3'
Mucin-1	5'-GACATCTTTCCAACCCAGGA-3' 5'-CTGCCGAAACCTCCTCATAG-3'
aPKC $\alpha$	5'-AGGATATCGATTGGGTGCAG-3' 5'-CATGAGGTCCCCTCCATTA-3'
aPKC $\zeta$	5'-CGGGACCTAAACTGGACAA-3' 5'-GATTTCGGGGCGATATAGT-3'
Notch 1	5'-GGTCGCAACTGTGAGAGTGA-3' 5'-GATTGCTGGCACATTCATTG-3'
Notch 2	5'-GGAGATCGACAACCGACAGT-3' 5'-GCGTTTCTTGACTCTCCAG-3'
Notch 3	5'-TGCCAGAGTTCAGTGGTGG-3' 5'-CACAGCAAATCGCCATC-3'
Notch 4	5'-CAAGCTCCCGTAGTCCTACTT-3' 5'-GACCCCCGTTGGAACAGAAAG-3'
Jagged 1	5'-GGTCCTGGATGACCAGTGTT-3' 5'-GTTTCGGTGGTAAGACCTGGA-3'
Dll 1	5'-TCAATGGAGGACGATGTTCA-3' 5'-ACCGGCACAGGTAAGAGTTG-3'
Hes 1	5'-GTGGTCCTAACGCAGTGC-3' 5'-ACAAAGGCGCAATCCAATATG-3'

## REFERENCES

- Boyer, D.F., Fujitani, Y., Gannon, M., Powers, A.C., Stein, R.W., and Wright, C.V. (2006). Complementation rescue of Pdx1 null phenotype demonstrates distinct roles of proximal and distal cis-regulatory sequences in pancreatic and duodenal expression. *Dev Biol* 298, 616-631.
- Corbetta, S., Gualdoni, S., Albertinazzi, C., Paris, S., Croci, L., Consalez, G.G., and de Curtis, I. (2005). Generation and characterization of Rac3 knockout mice. *Mol Cell Biol* 25, 5763-5776.
- Gao, N., White, P., Doliba, N., Golson, M.L., Matschinsky, F.M., and Kaestner, K.H. (2007). Foxa2 controls vesicle docking and insulin secretion in mature Beta cells. *Cell Metab* 6, 267-279.
- Lapierre, L.A., Tuma, P.L., Navarre, J., Goldenring, J.R., and Anderson, J.M. (1999). VAP-33 localizes to both an intracellular vesicle population and with occludin at the tight junction. *J Cell Sci* 112 ( Pt 21), 3723-3732.
- Makarova, O., Roh, M.H., Liu, C.J., Laurinec, S., and Margolis, B. (2003). Mammalian Crumbs3 is a small transmembrane protein linked to protein associated with Lin-7 (Pals1). *Gene* 302, 21-29.
- Masui, T., Long, Q., Beres, T.M., Magnuson, M.A., and MacDonald, R.J. (2007). Early pancreatic development requires the vertebrate Suppressor of Hairless (RBPJ) in the PTF1 bHLH complex. *Genes Dev* 21, 2629-2643.
- Sorokin, L.M., Conzelmann, S., Ekblom, P., Battaglia, C., Aumailley, M., and Timpl, R. (1992). Monoclonal antibodies against laminin A chain fragment E3 and their effects on binding to cells and proteoglycan and on kidney development. *Exp Cell Res* 201, 137-144.
- Suzuki, A., Yamanaka, T., Hirose, T., Manabe, N., Mizuno, K., Shimizu, M., Akimoto, K., Izumi, Y., Ohnishi, T., and Ohno, S. (2001). Atypical protein kinase C is involved in the evolutionarily conserved par protein complex and plays a critical role in establishing epithelia-specific junctional structures. *J Cell Biol* 152, 1183-1196.